Computer Methods and Programs in Biomedicine Update 8 (2025) 100216

Contents lists available at ScienceDirect

Computer Methods and Programs in Biomedicine Update

journal homepage:
www.sciencedirect.com/journal/computer-methods-and-programs-in-biomedicine-update

# Mathematical modeling of the impact of HPV vaccine uptake in reducing cervical cancer using a graph-theoretic approach via Caputo fractional-order derivatives

Sylas Oswald [a,e,*], Eunice Mureithi [a], Berge Tsanou [b,c], Michael Chapwanya [c], Crispin Kahesa [d], Kijakazi Mashoto [e]

[a] Department of Mathematics, University of Dar Es Salaam, P.O Box 35062, Dar Es Salaam, Tanzania
[b] Department of Mathematics & Computer Science, Faculty of Science, University of Dschang, P.O. Box 67, Dschang, Cameroon
[c] Department of Mathematics & Applied Mathematics, University of Pretoria, South Africa
[d] Ocean Road Cancer Institute (ORCI): Dar Es Salaam , Tanzania
[e] National Institute for Medical Research (NIMR), Headquarters: Dar Es Salaam , Tanzania

ARTICLE INFO

*Keywords:*
Mittag-Leffler
Trivial node
Irreducible
Self-loop
Memory effect
Predictor–corrector
Hyers–Ulam stability

ABSTRACT

Human papillomavirus (HPV) is a highly prevalent sexually transmitted infection and the primary cause of cervical cancer, which remains a leading cause of cancer-related mortality among women globally. Despite ongoing vaccination efforts, challenges such as latency, persistent infections, and imperfect vaccine coverage complicate disease control. In this study, we develop a novel fractional-order compartmental model using Caputo derivatives to capture the memory and non-local transmission effects inherent in HPV dynamics. We analyze the model's epidemiological properties by proving positivity, boundedness, and deriving the effective reproduction number ($\mathcal{R}_e$) via a Graph Theoretic approach. Stability of disease-free and endemic equilibria is established through Lyapunov theory, complemented by Hyers–Ulam stability to ensure robustness. Parameter estimation is performed using Markov Chain Monte Carlo (MCMC), and sensitivity analysis utilizes Partial Rank Correlation Coefficients (PRCC) to identify key drivers of transmission. Our results indicate that achieving 56% vaccination coverage with 45.5% efficacy can reduce $\mathcal{R}_e$ below one, supporting herd immunity. Numerical simulations demonstrate that vaccination coverage, timely treatment, and vaccine efficacy critically reduce infection prevalence and disease burden. Furthermore, higher fractional orders accelerate convergence to equilibrium without changing equilibrium values. This work lies in integrating fractional calculus with time-dependent vaccination and treatment controls to realistically model HPV progression and intervention impact. This approach provides a more accurate representation of HPV transmission dynamics, especially the long-term memory effects, thereby offering valuable insights for optimizing public health strategies.

## 1. Introduction

Human papillomavirus (HPV) is a highly prevalent sexually transmitted infection, with most cases resolving naturally. However, persistent infection with high-risk strains, notably HPV types 16 and 18, is strongly associated with the development of cervical cancer. This poses a significant health threat in low- and middle-income countries (LMICs) such as Tanzania, where access to screening and treatment is limited and the burden of HPV-related disease remains disproportionately high [1,2].

Globally, cervical cancer ranks as the fourth most common cancer among women, accounting for approximately 661,021 new cases and 348,189 deaths annually. Over 85% of these cases occur in LMICs. In Tanzania alone, around 14.5 million women aged 15–49, the age group most at risk face an HPV infection rate of at least 42.2%, leading to approximately 4,115 new cervical cancer cases each year [1,3,4]. In response, the Tanzanian government has implemented HPV vaccination programs targeting adolescent girls, supported by WHO and Gavi, to reduce the incidence of cervical cancer [2,5–7].

Mathematical modeling has become an essential tool for understanding HPV transmission dynamics and guiding vaccination strategies. For example, Liu et al. [8] used a compartmental model to assess the combined effects of vaccination and contact reduction on cervical cancer risk.

* Corresponding author at: Department of Mathematics, University of Dar Es Salaam, P.O Box 35062, Dar Es Salaam, Tanzania.
*E-mail address:* sylasossy2023@gmail.com (S. Oswald).

https://doi.org/10.1016/j.cmpbup.2025.100216
Received 20 May 2025; Received in revised form 29 July 2025; Accepted 1 August 2025
Available online 18 August 2025

Oswald et al. [9] emphasized the importance of vaccinating both young girls and older women to achieve herd immunity, recommending a minimum coverage of 55.83%. Similarly, Choi et al. [10] projected that raising vaccination coverage to 80% could prevent over 5,000 oropharyngeal cancer cases and save approximately 0.57 billion USD in healthcare costs.

Despite ongoing efforts to promote the HPV vaccine, vaccination rates remain suboptimal, particularly in low-resource settings. For instance, Choi et al. [10] demonstrated that increasing HPV vaccination coverage to 80% could prevent over 5,000 cases of oropharyngeal cancer and save approximately 0.57 billion USD in healthcare costs. However, behavioral challenges such as individuals' failure to retain preventive knowledge or comply with vaccination schedules continue to hinder widespread protection. This calls for more sophisticated tools to model not only current but also past influences on disease transmission.

Traditional integer-order models, which rely only on the current system state, often fail to capture memory-dependent and hereditary effects intrinsic to many infectious diseases, including HPV. Since HPV exhibits latency and long-term persistence, models that ignore historical effects may underestimate the disease burden or misrepresent intervention efficacy. Fractional-order models, particularly those employing Caputo derivatives, address this limitation by incorporating memory and capturing the cumulative impact of past exposures, infections, and vaccinations [11–14].

Fractional-order approaches have already demonstrated their relevance in modeling various infections. El-Mesady et al. [15] applied a fractional-order model with control measures to tuberculosis, effectively illustrating how memory effects influence disease progression and intervention outcomes. In the context of HPV, Ali et al. [16] introduced a fractional model capturing the link between HPV infection and cervical cancer, highlighting the influence of prior infections and vaccinations on current dynamics. Similarly, Simelane et al. [17] emphasized the value of Caputo-based modeling in evaluating public health education and vaccination strategies. These studies underscore the need for memory-integrated models when evaluating persistent infections like HPV.

Building on the foundational work of Oswald et al. [9], this study extends their classical HPV transmission model by incorporating Caputo fractional-order derivatives to account for memory effects and biological persistence. Unlike traditional ODE-based models, the fractional framework offers a more realistic representation of HPV latency, partial vaccine efficacy, and disease progression. This extension enhances predictive accuracy and supports more effective public health strategies for HPV control and cervical cancer prevention.

Based on this foundational model, our study further introduces a novel fractional-order HPV model that explicitly incorporates both vaccination and treatment as time-dependent control variables. Unlike previous models that emphasized either theoretical properties or isolated interventions, our approach addresses the real-world complexity of HPV management by evaluating the effectiveness of combined control strategies over time. Inspired by the optimal control frameworks in Elsonbaty et al. [18] and El-Mesady et al. [19], this model integrates delayed immune responses and vaccine memory effects, providing a flexible and more accurate tool for policy development.

This modeling approach is especially relevant in low- and middle-income countries (LMICs), such as Tanzania, where limited resources and delayed health system responses pose significant challenges to HPV control. Classical models often fail to capture these contextual realities. In contrast, our fractional framework—supported by prior successes in modeling diseases like chickenpox [20], COVID-19 [21], and rabies [22,23]—offers a robust mechanism for analyzing long-term disease dynamics. By evaluating the durability and optimal timing of interventions, this model aims to guide sustainable and context-sensitive public health strategies in resource-constrained settings.

### 1.0.1. *Basic properties of the fractional calculus*

In this section, we introduce a fractional-order model to investigate the transmission dynamics of Human Papillomavirus (HPV), incorporating both vaccination and treatment strategies. The model is formulated within the framework of Fractional Calculus (FC), specifically employing the Caputo derivative. The Caputo fractional derivative of order $\alpha$ is defined by the expressions in Definitions 1–8 and Lemma 1.1, which provide the necessary mathematical basis for the model. This approach enables a more comprehensive representation of disease propagation, capturing memory effects and non-local interactions within the population.

**Definition 1** (*[11,14,24,25]*)**.** The left and right Riemann–Liouville fractional (R-LF) integrals $I^{\alpha}_{a^+}f$ and $I^{\alpha}_{b^-}f$ of order $\alpha \in \mathbb{C}$ $(\Re(\alpha) > 0)$ are defined as:

$$I^{\alpha}_{a^+}f(t) = \frac{1}{\Gamma(\alpha)}\int_a^t (t-s)^{\alpha-1} f(s)\,ds, \tag{1}$$

$$I^{\alpha}_{b^-}f(t) = \frac{1}{\Gamma(\alpha)}\int_t^b (s-t)^{\alpha-1} f(s)\,ds, \tag{2}$$

where $\Gamma(.)$ is the Euler gamma function.

**Definition 2** (*[22,23,25]*)**.** The left and right Riemann–Liouville fractional derivatives $D^{\alpha}_{a^+}f$ and $D^{\alpha}_{b^-}f$ of order $\alpha \in \mathbb{C}$ $(\Re(\alpha) > 0)$ are defined as:

$$(D^{\alpha}_{a^+}f)(t) = \left(\frac{d}{dt}\right)^n (I^{n-\alpha}_{a^+}f)(t) = \frac{1}{\Gamma(n-\alpha)}\left(\frac{d}{dt}\right)^n \int_a^t \frac{f(s)}{(t-s)^{\alpha-n+1}}\,ds, \tag{3}$$

$$(D^{\alpha}_{b^-}f)(t) = \left(-\frac{d}{dt}\right)^n (I^{n-\alpha}_{b^-}f)(t) = \frac{1}{\Gamma(n-\alpha)}\left(-\frac{d}{dt}\right)^n \int_t^b \frac{f(s)}{(s-t)^{\alpha-n+1}}\,ds, \tag{4}$$

where $n = \Re(\alpha) + 1$ is the highest integer less than or equal to $\Re(\alpha)$.

**Definition 3** (*Linearity Property [26–28]*)**.** Let $f(t), g(t) : [a,b] \to \mathbb{R}$ be such that ${}^{C}_{a}D^{\alpha}_{t}f(t)$ and ${}^{C}_{a}D^{\alpha}_{t}g(t)$ exist almost everywhere, and let $k_1, k_2 \in \mathbb{R}$. Then, ${}^{C}_{a}D^{\alpha}_{t}(k_1 f(t)) + {}^{C}_{a}D^{\alpha}_{t}(k_2 g(t))$ exists everywhere, and

$${}^{C}_{a}D^{\alpha}_{t}\left\{k_1 f(t) + k_2 g(t)\right\} = k_1 {}^{C}_{a}D^{\alpha}_{t}f(t) + k_2 {}^{C}_{a}D^{\alpha}_{t}g(t). \tag{5}$$

**Definition 4** (*Caputo Derivative of a Constant [25,26,29,30]*)**.** The fractional derivative of a constant function $f(t) = c$ is zero, that is, ${}^{C}_{a}D^{\alpha}_{t}c = 0$. Let us consider the following general type of fractional differential equation involving the Caputo derivative:

$${}^{C}_{a}D^{\alpha}_{t}x(t) = f\,(t, x(t))\,, \quad \alpha \in (0,1), \tag{6}$$

with initial condition $x_0 = x(t_0)$.

**Definition 5** ([19,25,31]). Let $f(t) \in \mathbb{C}^n([0,\infty),\mathbb{R})$ be a function. The left and right fractional derivative in the Caputo sense ${}^{C}D^{\alpha}_{a^+}f$ and ${}^{C}D^{\alpha}_{b^-}f$ of order $n-1 < \alpha \le n$ where $n \in \mathbb{N}$ and $\alpha \in \mathbb{C}$ ($\Re(\alpha) > 0$) are defined:

$$ {}^{C}D^{\alpha}_{a^+}f(t) = \frac{1}{\Gamma(n-\alpha)} \int_a^t \frac{f^{(n)}(s)}{(t-s)^{\alpha-n+1}}\, ds, \tag{7} $$

$$ {}^{C}D^{\alpha}_{b^-}f(t) = \frac{(-1)^n}{\Gamma(n-\alpha)} \int_t^b \frac{f^{(n)}(s)}{(s-t)^{\alpha-n+1}}\, ds, \tag{8} $$

where $f^{(n)}(t)$ represents the $n$th derivative of $f(t)$, and ${}^{C}D^{\alpha}_{t}f(t)$ approaches $f'(t)$ as $\alpha \to 1$.

**Definition 6** ([19,31,32] *Generalized Mean Value Theorem*). Let $f(t) \in C[a,b]$ and ${}^{C}_{0}D^{\alpha}_{t}f(t) \in C[a,b]$ for $0 < \alpha \le 1$. Then:

$$ f(t) = f(a) + \frac{1}{\Gamma(\alpha)} {}^{C}_{0}D^{\alpha}_{\xi} f(\xi)(t-a)^{\alpha}, \tag{9} $$

where $a \le \xi \le t$ and $\forall_t \in [a,b]$.

**Definition 7** ([14,25] *Mittag-Leffler Function*). For $\alpha, \beta \in \mathbb{C}$ ($\Re(\alpha) > 0$), the Mittag-Leffler function described by infinite power series defined as:

$$ E_{\alpha,\beta}(z) = \sum_{k=0}^{\infty} \frac{z^k}{\Gamma(\alpha k + \beta)}, \text{when } \beta = 1, \text{ it is written as } \quad E_{\alpha}(z) \overset{\text{def}}{=} E_{\alpha,1}(z) = \sum_{k=0}^{\infty} \frac{z^k}{\Gamma(\alpha k + 1)}. \tag{10} $$

**Definition 8** ([25,33,34]). Let $F(s)$ be the Laplace transform of the function $f(t)$. Then, the Laplace transform of the Caputo derivative is given by

$$ (\mathcal{L}\, {}^{C}D^{\alpha}_{0^+} f(t))(s) = s^{\alpha}(\mathcal{L}f(t))(s) - \sum_{j=0}^{l-1} d_j s^{\alpha-j-1}, \tag{11} $$

where $l-1 < \alpha \le l$, $\quad l \in \mathbb{N}$, and with $d_j = f^{(j)}(0) \quad (j = 0, 1, \ldots, l-1)$.

**Lemma 1.1** (*See* [26,35]). *Let $x(\cdot)$ be a continuous and differentiable function with $x(t) \in \mathbb{R}^+$. Then, for any time instant $t \ge t_0$, one has*

$$ {}^{C}_{0}D^{\alpha}_{t}\left(x(t) - x^* - x^* \ln\left(\frac{x(t)}{x^*}\right)\right) \le \left(1 - \frac{x^*}{x(t)}\right) {}^{C}_{0}D^{\alpha}_{t} x(t), \quad x^* \in \mathbb{R}^+, \forall \alpha \in (0,1). \tag{12} $$

## 2. Epidemiological model formulation

Building on the foundational work of Oswald et al. [9], this study develops an enhanced mathematical framework to analyze the transmission dynamics of Human Papillomavirus (HPV) by incorporating Caputo fractional-order derivatives, the model effectively captures memory effects inherent in disease progression, thereby providing a more realistic representation of the biological persistence of HPV.

The population at time $t$ is denoted by $N(t) = N_f(t) + N_m(t)$, where $N_f(t)$ and $N_m(t)$ represent the total female and male subpopulations, respectively. The female population is subdivided into six epidemiological compartments: susceptible $S_f(t)$, vaccinated $V(t)$, exposed $E_f(t)$, infectious $I_f(t)$, cervical cancer cases $C(t)$, and recovered $R_f(t)$. Meanwhile, the male population is categorized into four compartments: susceptible $S_m(t)$, exposed $E_m(t)$, infectious $I_m(t)$, and recovered $R_m(t)$.

Recruitment into the population occurs through three pathways: females who have not been successfully vaccinated, comprising a proportion $(1-\phi)\pi^{\alpha}_{f}$, enter the susceptible class $S_f$; those successfully vaccinated, representing a fraction $\phi\pi^{\alpha}_{f}$, join the vaccinated class $V$. Males are recruited at a rate $\pi^{\alpha}_{m}$ directly into the susceptible class $S_m$.

Transmission of HPV occurs through effective sexual contact between susceptible individuals and their exposed or infectious partners. The force of infection for females is given by: $\lambda^{\alpha}_{m} = \dfrac{\zeta^{\alpha}_{m\to f}(\psi^{\alpha}_{m}E_m + I_m)}{N_m}$, where $\zeta^{\alpha}_{m\to f}$ denotes the probability of transmission from males to females, and $\psi^{\alpha}_{m} \in [0,1)$ accounts for the reduced infectivity of exposed males. Similarly, the force of infection for males is defined as: $\lambda^{\alpha}_{f} = \dfrac{\zeta^{\alpha}_{f\to m}(\psi^{\alpha}_{f}E_f + I_f)}{N_f}$, where $\zeta^{\alpha}_{f\to m}$ and $\psi^{\alpha}_{f}$ are the corresponding transmission probability and infectivity modifier from females to males.

Susceptible individuals $S_f$ and $S_m$ may become exposed at rates $\lambda^{\alpha}_{m}S_f$ and $\lambda^{\alpha}_{f}S_m$, respectively. Vaccinated females $V$, who have partial immunity, may still become infected at rate $(1-\delta)\lambda^{\alpha}_{m}V, \quad (0 < \delta < 1)$ entering the exposed class $E_f$.

Exposed individuals $E_f$ and $E_m$ progress to the infectious stages $I_f$ and $I_m$ at rates $\gamma^{\alpha}_{f}$ and $\gamma^{\alpha}_{m}$, respectively. Infected females $I_f$ may either recover at rate $\eta\xi^{\alpha}_{f}I_f$, moving to $R_f$, or progress to cervical cancer at rate $(1-\eta)\xi^{\alpha}_{f}I_f$. Cervical cancer cases $C$ may recover following treatment at rate $\tau^{\alpha}C$, or die due to disease and natural causes at rate $(\mu^{\alpha} + d^{\alpha})C$. Infected males $I_m$ recover at rate $\xi^{\alpha}_{m}I_m$, transitioning to the recovered class $R_m$.

All compartments are subject to natural mortality at rate $\mu^{\alpha}$. The model captures both direct and cross-gender transmission dynamics, where individuals may acquire infection from partners of the opposite sex, contributing to the persistence and spread of HPV in the population.

This formulation incorporates two key public health interventions: (i) vaccination of females to reduce infection and cervical cancer incidence, and (ii) treatment of individuals diagnosed with cervical cancer. Although the vaccine reduces infection risk, it is assumed to be imperfect, allowing for breakthrough infections among vaccinated females. Additionally, due to limited epidemiological evidence, penile cancer-related mortality in males is not considered.

The transmission dynamics are governed by a system of fractional differential equations and are illustrated in Fig. 1. Definitions of all model parameters and their epidemiological interpretations are provided in Table 1, supporting both theoretical analysis and numerical simulations.

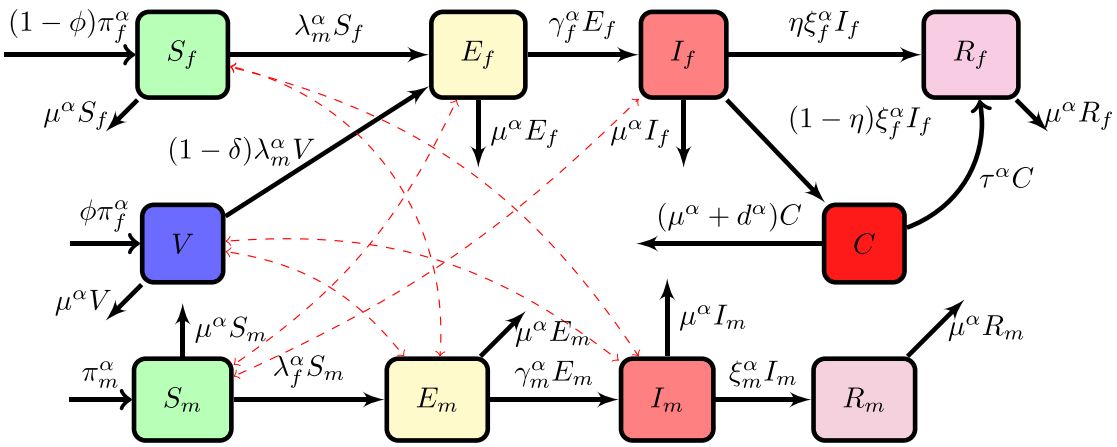


**Fig. 1.** Transition diagram for the HPV vaccination and treatment.

**Table 1**
Model variables and parameters along with their epidemiological interpretations in the fractional-order HPV transmission model 1.

| Symbol | Biological/Epidemiological Description |
|---|---|
| $S_f(t)$, $S_m(t)$ | Number of susceptible females and males at time $t$ |
| $V(t)$ | Population of vaccinated females at time $t$ (with partial immunity) |
| $E_f(t)$, $E_m(t)$ | Females and males in the latent/exposed stage following infection |
| $I_f(t)$, $I_m(t)$ | Infected individuals (females and males) capable of transmitting HPV |
| $C(t)$ | Females who have developed cervical cancer due to persistent HPV infection |
| $R_f(t)$, $R_m(t)$ | Individuals (female and male) who have recovered from HPV infection |
| $\lambda_f^\alpha$, $\lambda_m^\alpha$ | Force of infection for males and females, respectively |
| $\pi_f^\alpha$, $\pi_m^\alpha$ | Recruitment rate of sexually active females and males (fractional-order adjusted) |
| $\delta$ | Degree of protection conferred by the HPV vaccine (efficacy level) |
| $\phi$ | Proportion of newly recruited females receiving vaccination |
| $\tau^\alpha$ | Rate at which cervical cancer cases receive treatment (fractional-order) |
| $\xi_m^\alpha$, $\xi_f^\alpha$ | Removal rate of infected males and females from the infectious class |
| $\eta$, $1-\eta$ | Fraction of infected females who recover ($\eta$) or progress to cervical cancer ($1-\eta$) |
| $\psi_f$, $\psi_m$ | Infectivity modification factors for exposed females and males |
| $\mu^\alpha$ | Natural mortality rate applicable to all individuals (fractional-order) |
| $d^\alpha$ | Disease-induced mortality rate among cervical cancer patients |
| $\zeta_{f\to m}^\alpha$, $\zeta_{m\to f}^\alpha$ | Per-contact probability of HPV transmission from female to male and vice versa |
| $\gamma_f^\alpha$, $\gamma_m^\alpha$ | Rate of symptom progression in infected females and males |

Model (13) presents the compartmental structure of the HPV transmission model, which is formulated using Caputo fractional derivatives. In this formulation, ${}_0^C D_t^\alpha$ denotes the Caputo derivative of order $\alpha$, where $\alpha \in (0,1)$. The model delineates the dynamics among susceptible, vaccinated, exposed, infectious, and recovered individuals, incorporating the impacts of both vaccination and treatment strategies.

$$
\begin{cases}
{}_{t_0}^C D_t^\alpha S_f(t) &= (1-\phi)\pi_f^\alpha - (\mu^\alpha + \lambda_m^\alpha)S_f(t),\\
{}_{t_0}^C D_t^\alpha V(t) &= \phi\pi_f^\alpha - \mu^\alpha V(t) - (1-\delta)\lambda_m^\alpha V(t),\\
{}_{t_0}^C D_t^\alpha E_f(t) &= \lambda_m^\alpha S_f(t) + (1-\delta)\lambda_m^\alpha V(t) - (\mu^\alpha + \gamma_f^\alpha)E_f(t),\\
{}_{t_0}^C D_t^\alpha I_f(t) &= \gamma_f^\alpha E_f(t) - (\mu^\alpha + \xi_f^\alpha)I_f(t),\\
{}_{t_0}^C D_t^\alpha R_f(t) &= \eta\xi_f^\alpha I_f(t) + \tau^\alpha C(t) - \mu^\alpha R_f(t),\\
{}_{t_0}^C D_t^\alpha C(t) &= (1-\eta)\xi_f^\alpha I_f(t) - (\mu^\alpha + d^\alpha + \tau^\alpha)C(t),\\
{}_{t_0}^C D_t^\alpha S_m(t) &= \pi_m^\alpha - (\mu^\alpha + \lambda_f^\alpha)S_m(t),\\
{}_{t_0}^C D_t^\alpha E_m(t) &= \lambda_f^\alpha S_m(t) - (\mu^\alpha + \gamma_m^\alpha)E_m(t),\\
{}_{t_0}^C D_t^\alpha I_m(t) &= \gamma_m^\alpha E_m(t) - (\mu^\alpha + \xi_m^\alpha)I_m(t),\\
{}_{t_0}^C D_t^\alpha R_m(t) &= \xi_m^\alpha I_m(t) - \mu^\alpha R_m(t),
\end{cases}
\tag{13}
$$

where, $\lambda_m^\alpha = \zeta_{m\to f}^\alpha \dfrac{(\psi_m^\alpha E_m + I_m)}{N_m}$ and, $\lambda_f^\alpha = \zeta_{f\to m}^\alpha \dfrac{(\psi_f^\alpha E_f + I_f)}{N_f}$.

### 2.1. Theoretical analysis of the Fractional System Model (FSM)

#### 2.1.1. Positivity and boundedness of solutions

For the FSM (13) to be epidemiologically meaningful, it is vital to establish the positivity of the solution, whenever the ICs and all parameters are assumed to be positive, we introduce corollary as discussed by [16,18,19,31,36].

**Corollary 1.** *Let $f(t) \in C[t_0, T]$ and ${}_{t_0}^C D_t^\alpha f(t) \in C[t_0, T]$ for $0 < \alpha \le 1$. It is mathematically meaningful from 4 together with 6, that*

*(i) If* ${}_{t_0}^{C}D_t^{\alpha} f(t) \geq 0, \quad \forall t \in (t_0, T]$, *then* $f(t)$ *is non-decreasing* $\quad \forall t \in (t_0, T]$.
*(ii) If* ${}_{t_0}^{C}D_t^{\alpha} f(t) \leq 0, \quad \forall t \in (t_0, T]$, *then* $f(t)$ *is non-increasing* $\quad \forall t \in (t_0, T]$.

**Theorem 1.** *For the model FSM (13), the region*

$$\Omega_+ = \{(S_f, V, E_f, I_f, R_f, C, S_m, E_m, I_m, R_m) \mid S_f > 0,\ V \geq 0,\ E_f \geq 0,\ I_f \geq 0, R_f \geq 0,\ C \geq 0,\ S_m > 0,\ E_m \geq 0,\ I_m \geq 0,\ R_m \geq 0\}$$

*is a positive invariant.*

**Proof.** We now demonstrate that the region $\Omega_+$ for the FSM (13) remains positive over time.

$$\begin{aligned}
{}_{t_0}^{C}D_t^{\alpha} S_f(t)|_{S_f=0} &= (1-\phi)\pi_f^{\alpha} > 0,\\
{}_{t_0}^{C}D_t^{\alpha} V(t)|_{V=0} &= \phi\pi_f^{\alpha} \geq 0,\\
{}_{t_0}^{C}D_t^{\alpha} E_f(t)|_{E_f=0} &= \lambda_m^{\alpha} S_f(t) + (1-\delta)\lambda_m^{\alpha} V(t) \geq 0,\\
{}_{t_0}^{C}D_t^{\alpha} I_f(t)|_{I_f=0} &= \gamma_f^{\alpha} E_f(t) \geq 0,\\
{}_{t_0}^{C}D_t^{\alpha} R_f(t)|_{R_f=0} &= \eta\xi_f^{\alpha} I_f(t) + \tau^{\alpha} C(t) \geq 0,\\
{}_{t_0}^{C}D_t^{\alpha} C(t)|_{C=0} &= (1-\eta)\xi_f^{\alpha} I_f(t) \geq 0,\\
{}_{t_0}^{C}D_t^{\alpha} S_m(t)|_{S_m=0} &= \pi_m^{\alpha} > 0,\\
{}_{t_0}^{C}D_t^{\alpha} E_m(t)|_{E_m=0} &= \lambda_f^{\alpha} S_m(t) \geq 0,\\
{}_{t_0}^{C}D_t^{\alpha} I_m(t)|_{I_m=0} &= \gamma_m^{\alpha} E_m(t) \geq 0,\\
{}_{t_0}^{C}D_t^{\alpha} R_m(t)|_{R_m=0} &= \xi_m^{\alpha} I_m(t) \geq 0.
\end{aligned} \tag{14}$$

This implies that all solutions of FSM (13) remain within the positively invariant region $\Omega_+$, as established by Corollary 1. Since FSM (13) describes the dynamics of a human population, it is sufficient to show that its solutions are bounded and non-decreasing $\forall t \geq 0$. □

To demonstrate the solution's boundedness, the following theorem is presented:

**Theorem 2.** *Model (13) has unique and non-decreasing solutions which turn into region* $\Omega_+$ *as* $t \to \infty$, *such that* $\Omega_+ = \{ (S_f, V, E_f, I_f, R_f, C, S_m, E_m, I_m, R_m) \in R_+^{10} | \ (S_f + V + E_f + I_f + R_f + C + S_m + E_m + I_m + R_m) = N \leq \frac{\pi_f^{\alpha} + \pi_m^{\alpha}}{\mu^{\alpha}} \}$ *is positively invariant set for FSM.*

**Proof.** The work [15,20,21,37–39] guarantees the positivity of the solution to the FSM (13) on the interval $[0, \infty)$. By summing all equations of system (13), one gets:

$${}_{0}^{C}D_t^{\alpha} N(t) = {}_{0}^{C}D_t^{\alpha} N_f(t) + {}_{0}^{C}D_t^{\alpha} N_m(t) = \pi_f^{\alpha} + \pi_m^{\alpha} - \mu^{\alpha} N(t) - (\eta\xi_f^{\alpha} I_f(t) + d^{\alpha} C(t)) \leq \pi_f^{\alpha} + \pi_m^{\alpha} - \mu^{\alpha} N(t). \tag{15}$$

Utilizing Definition 8, the Laplace transform of (15) is given by:

$${}_{0}^{C}D_t^{\alpha} N(t) \leq \pi_f^{\alpha} + \pi_m^{\alpha} - \mu^{\alpha} N(t) \implies s^{\alpha+1}\mathcal{L}(N(t)) - s^{\alpha} N(0) \leq \pi_f^{\alpha} + \pi_m^{\alpha} - \mu^{\alpha} s(\mathcal{L}N(t)) \tag{16}$$

Combining and rearranging like terms leads to

$$(\mathcal{L}N(t)) \leq \frac{\pi_f^{\alpha} + \pi_m^{\alpha}}{s^{\alpha+1} + s\mu^{\alpha}} + \frac{s^{\alpha} N(0)}{s^{\alpha+1} + s\mu^{\alpha}} \implies \left(\pi_f^{\alpha} + \pi_m^{\alpha}\right) \frac{s^{-1}}{s^{\alpha} + \mu^{\alpha}} + N(0) \frac{s^{\alpha-1}}{s^{\alpha} + \mu^{\alpha}} \tag{17}$$

Applying the inverse Laplace transform together with Definition 8 leads to

$$\begin{aligned}
N(t) &\leq \mathcal{L}^{-1}\left\{ \left(\pi_f^{\alpha} + \pi_m^{\alpha}\right) \frac{s^{-1}}{s^{\alpha} + \mu^{\alpha}} + N(0) \frac{s^{\alpha-1}}{s^{\alpha} + \mu^{\alpha}} \right\}\\
&\leq \left(\pi_f^{\alpha} + \pi_m^{\alpha}\right) t^{\alpha} E_{\alpha,\alpha+1}(-\mu^{\alpha} t^{\alpha}) + N(0) E_{\alpha,1}(-\mu^{\alpha} t^{\alpha})\\
&\leq \frac{\left(\pi_f^{\alpha} + \pi_m^{\alpha}\right)}{\mu^{\alpha}} \mu^{\alpha} t^{\alpha} E_{\alpha,\alpha+1}(-\mu^{\alpha} t^{\alpha}) + N(0) E_{\alpha,1}(-\mu^{\alpha} t^{\alpha})\\
&\leq \max\left\{ \frac{\pi_f^{\alpha} + \pi_m^{\alpha}}{\mu^{\alpha}}, N(0) \right\} \left(\mu^{\alpha} t^{\alpha} E_{\alpha,\alpha+1}(-\mu^{\alpha} t^{\alpha}) + E_{\alpha,1}(-\mu^{\alpha} t^{\alpha})\right)
\end{aligned} \tag{18}$$

Based on the asymptotic behavior of the Mittag–Leffler function with Definition 7, we let $Q = \frac{\pi_f^{\alpha} + \pi_m^{\alpha}}{\mu^{\alpha}}$ so that

$$\max\{Q, N(0)\} = \frac{Q}{\Gamma(1)} = Q \implies N(t) \leq \frac{\pi_f^{\alpha} + \pi_m^{\alpha}}{\mu^{\alpha}}. \tag{19}$$

Eq. (19) establishes that the proposed fractional-order system is epidemiologically valid, as it is mathematically well-posed and guarantees that all solutions to the HPV model, once initialized, remain within the feasible region. This confirms that the FSM (13) provides a meaningful epidemiological interpretation, particularly when all state variables are positive. As a result, the solution is constrained within bounds and attracts all trajectories in the domain $\Omega$. Therefore, the dynamics of the FSM (13) can be effectively analyzed within the domain $\Omega$ as it is illustrated in Fig. 2. □

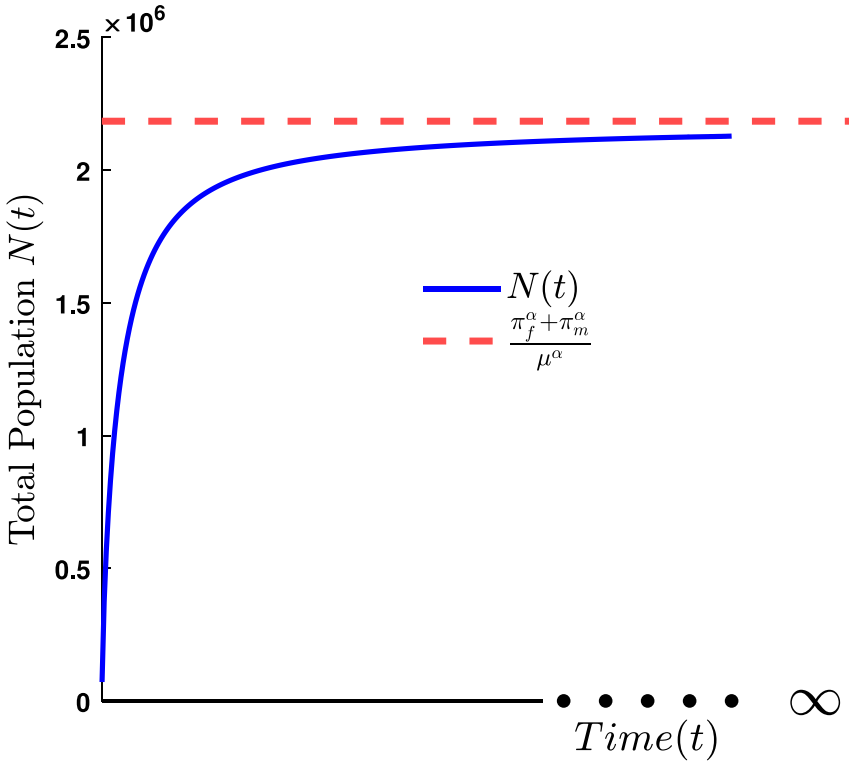


**Fig. 2.** As $t \to \infty$, $N(t) \leq \frac{\pi_f^{\alpha}+\pi_m^{\alpha}}{\mu^{\alpha}}$.

### 2.2. Papillomavirus-free equilibrium and HPV reproduction number

In the papillomavirus-free context, the community is free from HPV infection, with the infected class taking a value of zero. Thus, the equilibrium point is given by:

$$PFE = \left( \frac{(1-\phi)\pi_f^{\alpha}}{\mu^{\alpha}}, \quad \frac{\phi\pi_f^{\alpha}}{\mu^{\alpha}}, \quad 0, \quad 0, \quad 0, \quad 0, \quad \frac{\pi_m^{\alpha}}{\mu^{\alpha}}, \quad 0, \quad 0, \quad 0 \right)$$

The effective reproduction number, $\mathcal{R}_e$, is a key metric in both medicine and epidemiology that helps evaluate the effectiveness of control strategies by measuring the average number of secondary infections generated by a single infected individual, as previously discussed in [9,40–43]. To fully understand disease transmission, it is essential to account for the influence of prior infections, which is captured by the model's memory effect. By incorporating the Caputo derivative, this model improves its representation of the transmission process by considering the historical impact of earlier infections on ongoing spread.

Additionally, $\mathcal{R}_e$ serves as a critical threshold parameter that determines whether HPV transmission will eventually diminish or persist. Specifically, when $\mathcal{R}_e \leq 1$, the infection's spread decreases, while $\mathcal{R}_e > 1$ enables continued transmission, heightening the risk of cervical cancer. To accurately compute $\mathcal{R}_e$, the model applies a Graph-Theoretic (GT) approach with a $\mathbb{GT}$-based Gaussian elimination method, as described in [44–46].

**Theorem 3.** *Let $F$ be a non-negative, non-zero matrix, and $V$ a non-singular M-matrix, with the assumption that the matrix $F-V$ is irreducible. Under these conditions, the effective reproduction number is defined as $\mathcal{R}_e = \rho(FV^{-1})$, where $\rho$ represents the spectral radius and $\mathcal{R}_e > 0$. Additionally, $\mathcal{R}_e$ corresponds to the reciprocal of the smallest positive solution, $x$, to the equation* $\det(Fx - V) = 0$.

**Proof.** Given the assumptions, $FV^{-1}$ is a non-negative, non-zero matrix. As noted by Li and Schneider [47], the principal submatrix corresponding to the non-zero rows of $F$ is irreducible. Consequently, $\lambda = \rho(FV^{-1}) > 0$ represents the largest positive eigenvalue of the matrix equation $\det(\lambda I - FV^{-1}) = 0$.

Since $V$ is non-singular and $\lambda > 0$, this equation can be reformulated as $\det(F\lambda^{-1} - V) = 0$, where $V - F\lambda^{-1}$ is a singular M-matrix. The smallest positive root is given by the reciprocal of $\lambda$, i.e., $\lambda^{-1}$. Therefore, the effective reproduction number is defined as $\mathcal{R}_e = \rho(FV^{-1})$. □

The approach outlined in [44–47] highlights that the $\mathbb{GT}$ method begins by separating new infections from other population dynamics. In this framework, $F$ is an $n \times n$ matrix, while $V$ is a non-singular $m \times m$ matrix. Both matrices are derived through fractional partial derivatives and evaluated at the system's equilibrium. The specific forms of $F$ and $V$ are provided herein:

$$F = \left[ \frac{\partial \mathcal{F}_i}{\partial(E_f, I_f, C, E_m, I_m)} \right]_{PFE} \text{ and } \quad V = \left[ \frac{\partial \mathcal{V}_i}{\partial(E_f, I_f, C, E_m, I_m)} \right]_{PFE} \tag{20}$$

$$\begin{cases} {}^{C}_{t_0}D^{\alpha}E_f(t) &= \lambda_m^{\alpha}S_f(t) + (1-\delta)\lambda_m^{\alpha}V(t) - (\mu^{\alpha}+\gamma_f^{\alpha})E_f(t), \\ {}^{C}_{t_0}D^{\alpha}_t I_f(t) &= \gamma_f^{\alpha}E_f(t) - (\mu^{\alpha}+\xi_f^{\alpha})I_f(t), \\ {}^{C}_{t_0}D^{\alpha}_t C(t) &= (1-\eta)\xi_f^{\alpha}I_f(t) - (\mu^{\alpha}+d^{\alpha}+\tau^{\alpha})C(t), \\ {}^{C}_{t_0}D^{\alpha}_t E_m(t) &= \lambda_m^{\alpha}S_m(t) - (\mu^{\alpha}+\gamma_m^{\alpha})E_m(t), \\ {}^{C}_{t_0}D^{\alpha}_t I_m(t) &= \gamma_m^{\alpha}E_m(t) - (\mu^{\alpha}+\xi_m^{\alpha})I_m(t), \end{cases} \tag{21}$$

Now, from (21) $\mathcal{F}_i$ and $\mathcal{V}_i$ are as follows

$$\mathcal{F}_i = \begin{pmatrix} \mathcal{F}_1 \\ \mathcal{F}_2 \\ \mathcal{F}_3 \\ \mathcal{F}_4 \\ \mathcal{F}_5 \end{pmatrix} = \begin{pmatrix} \lambda_m^{\alpha}(S_f(t)+(1-\delta)V(t)) \\ 0 \\ 0 \\ \lambda_f^{\alpha}S_m(t) \\ 0 \end{pmatrix} = \begin{pmatrix} \zeta_{m\to f}^{\alpha}\dfrac{(\psi_m E_m(t)+I_m(t))}{N_m(t)}(S_f+(1-\delta)V(t)) \\ 0 \\ 0 \\ \zeta_{f\to m}^{\alpha}\dfrac{(\psi_f E_f(t)+I_f(t))}{N_f(t)}S_m(t) \\ 0 \end{pmatrix}, \tag{22}$$

and

$$\mathcal{V}_i = \begin{pmatrix} \mathcal{V}_1 \\ \mathcal{V}_2 \\ \mathcal{V}_3 \\ \mathcal{V}_4 \\ \mathcal{V}_5 \end{pmatrix} = \begin{pmatrix} (\mu^{\alpha}+\gamma_f^{\alpha})E_f(t) \\ (\mu^{\alpha}+\xi_f^{\alpha})I_f(t) - \gamma_f^{\alpha}E_f(t) \\ (\mu^{\alpha}+d^{\alpha}+\tau^{\alpha})C(t) - (1-\eta)\xi_f^{\alpha}I_f(t) \\ (\mu^{\alpha}+\gamma_m^{\alpha})E_m(t) \\ (\mu^{\alpha}+\xi_m^{\alpha})I_m(t) - \gamma_m^{\alpha}E_m(t) \end{pmatrix}. \tag{23}$$

Now, evaluating the fractional partial derivative of $\mathcal{F}_i$ and $\mathcal{V}_i$ at $PFE$ with respect to $E_f, I_f, C, E_m$ and $I_m$ gives $F$ and $V$, that is then evaluated to obtain the matrix $Q = F\lambda^{-1} - V$ as follows:

$$Q = \begin{pmatrix} -(\mu^{\alpha}+\gamma_f^{\alpha}) & 0 & 0 & 0 & \dfrac{\zeta_{m\to f}^{\alpha}(2-\phi-\delta)\pi_f^{\alpha}}{\pi_m^{\alpha}}\lambda^{-1} \\ \gamma_f^{\alpha} & -(\mu^{\alpha}+\xi_f^{\alpha}) & 0 & 0 & 0 \\ 0 & (1-\eta)\xi_f^{\alpha} & -(\mu^{\alpha}+d^{\alpha}+\tau^{\alpha}) & 0 & 0 \\ \dfrac{\zeta_{f\to m}^{\alpha}\pi_m^{\alpha}}{\pi_f^{\alpha}}\lambda^{-1} & \dfrac{\zeta_{f\to m}^{\alpha}\pi_m^{\alpha}}{\pi_f^{\alpha}}\lambda^{-1} & \dfrac{\zeta_{f\to m}^{\alpha}\pi_m^{\alpha}}{\pi_f^{\alpha}}\lambda^{-1} & -(\mu^{\alpha}+\gamma_m^{\alpha}) & 0 \\ 0 & 0 & 0 & \gamma_m^{\alpha} & -(\mu^{\alpha}+\xi_m^{\alpha}) \end{pmatrix}. \tag{24}$$

### 2.3. Illustration of the matrix and digraph relationships in the model

The matrix $Q$ captures the transition dynamics between epidemiological compartments, with each element representing the rate of movement between states such as exposed, infected, and recovered individuals. The corresponding digraph visualizes these interactions, where nodes represent compartments, and directed edges denote transition rates. The nodes in the digraph, including $E_f$, $I_f$, $C$, $E_m$, and $I_m$, represent different disease states for females and males. Transition rates like $\gamma_f^{\alpha}$ and $\dfrac{\zeta_{m\to f}^{\alpha}(2-\phi-\delta)\pi_f^{\alpha}}{\pi_m^{\alpha}}$ illustrate disease progression and transmission dynamics. Self-loops on nodes indicate internal transitions, such as natural death and recovery, while off-diagonal elements capture the movement between compartments, like from exposed to infectious states as illustrated in Fig. 3.

#### 2.3.1. Digraph reduction and Gaussian elimination

Digraph reduction mimics Gaussian elimination on the matrix $F\lambda^{-1}-V$ by simplifying the system through the elimination of intermediate nodes, analogous to removing off-diagonal matrix elements. A node becomes trivial when its self-loop is normalized to $-1$, typically reflecting constant rates like natural mortality. Two key rules guide the process: (1) normalize incoming edges to create a trivial node, and (2) replace paths through that node with direct connections, preserving the determinant, as clearly described in detail in the work of Oswald et al. [9]. For example, node $I_m$ is reduced by dividing its incoming edges by $(\mu^{\alpha}+\xi_m^{\alpha})$ and updating the connections accordingly. Fig. 4 illustrates these structural transformations within the digraph.

The associated matrix is presented

$$M_1 = \begin{pmatrix} -(\mu^{\alpha}+\gamma_f^{\alpha}) & 0 & 0 & \dfrac{\zeta_{m\to f}^{\alpha}(2-\phi-\delta)\pi_f^{\alpha}\gamma_m^{\alpha}}{\pi_m^{\alpha}(\mu^{\alpha}+\xi_m^{\alpha})}\lambda^{-1} \\ \gamma_f^{\alpha} & -(\mu^{\alpha}+\xi_f^{\alpha}) & 0 & 0 \\ 0 & (1-\eta)\xi_f^{\alpha} & -(\mu^{\alpha}+d^{\alpha}+\tau^{\alpha}) & 0 \\ \dfrac{\zeta_{f\to m}^{\alpha}\pi_m^{\alpha}}{\pi_f^{\alpha}}\lambda^{-1} & \dfrac{\zeta_{f\to m}^{\alpha}\pi_m^{\alpha}}{\pi_f^{\alpha}}\lambda^{-1} & \dfrac{\zeta_{f\to m}^{\alpha}\pi_m^{\alpha}}{\pi_f^{\alpha}}\lambda^{-1} & -(\mu^{\alpha}+\gamma_m^{\alpha}) \end{pmatrix}. \tag{25}$$

The reduction procedure applied to node $E_m$ involves normalizing its self-loop weight $-(\mu^{\alpha}+\gamma_m^{\alpha})$ by dividing all incoming arc weights by $\mu^{\alpha}+\gamma_m^{\alpha}$. This transforms $E_m$ into a trivial node with a standardized loop weight of $-1$, consistent with digraph simplification principles. The reduced matrix corresponding to the digraph with node $E_m$ eliminated is as follows.

$$M_2 = \begin{pmatrix} -(\mu^{\alpha}+\gamma_f^{\alpha}) + \dfrac{\zeta_{f\to m}^{\alpha}\zeta_{m\to f}^{\alpha}(2-\phi-\delta)\gamma_m^{\alpha}}{(\mu^{\alpha}+\xi_m^{\alpha})(\mu^{\alpha}+\gamma_m^{\alpha})}\lambda^{-2} & 0 & \dfrac{\zeta_{f\to m}^{\alpha}\zeta_{m\to f}^{\alpha}(2-\phi-\delta)\gamma_m^{\alpha}}{(\mu^{\alpha}+\xi_m^{\alpha})(\mu^{\alpha}+\gamma_m^{\alpha})}\lambda^{-2} \\ \gamma_f^{\alpha} & -(\mu^{\alpha}+\xi_f^{\alpha}) & 0 \\ 0 & (1-\eta)\xi_f^{\alpha} & -(\mu^{\alpha}+d^{\alpha}+\tau^{\alpha}) \end{pmatrix}. \tag{26}$$

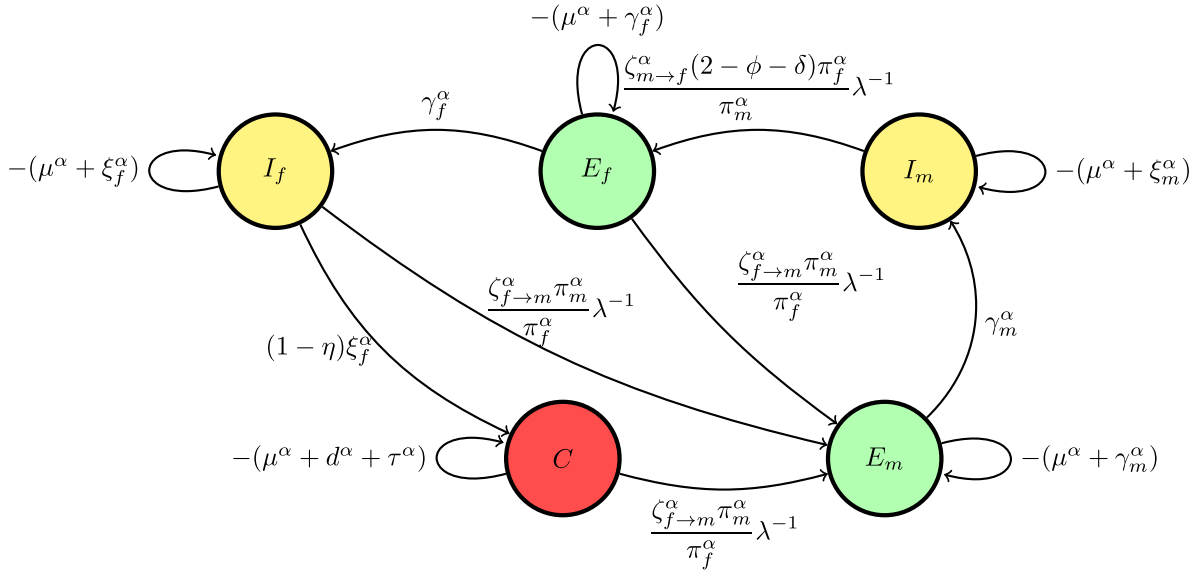


**Fig. 3.** (**A***) Digraph representation of $F\lambda^{-1}-V$.

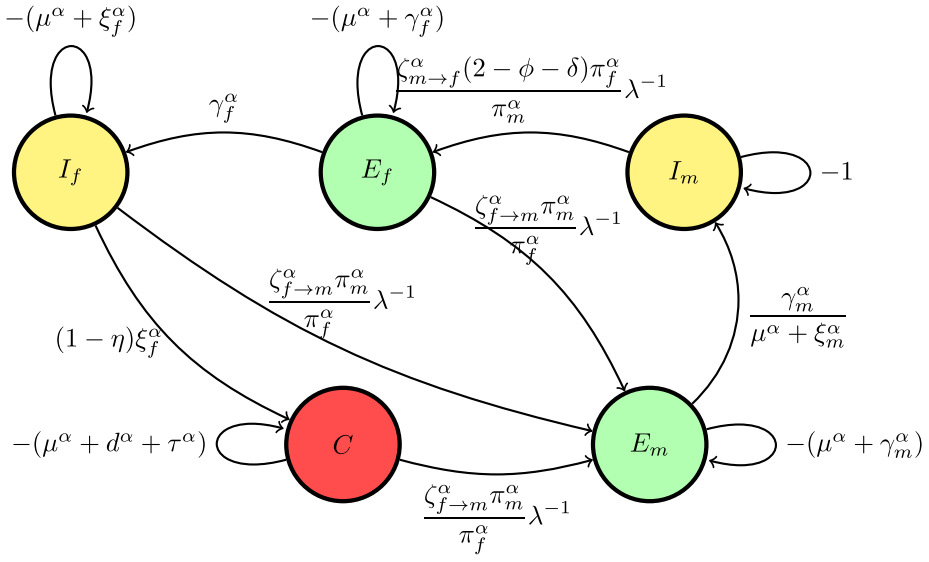


**Fig. 4.** (**A**) Creating a trivial node at node $I_m$.

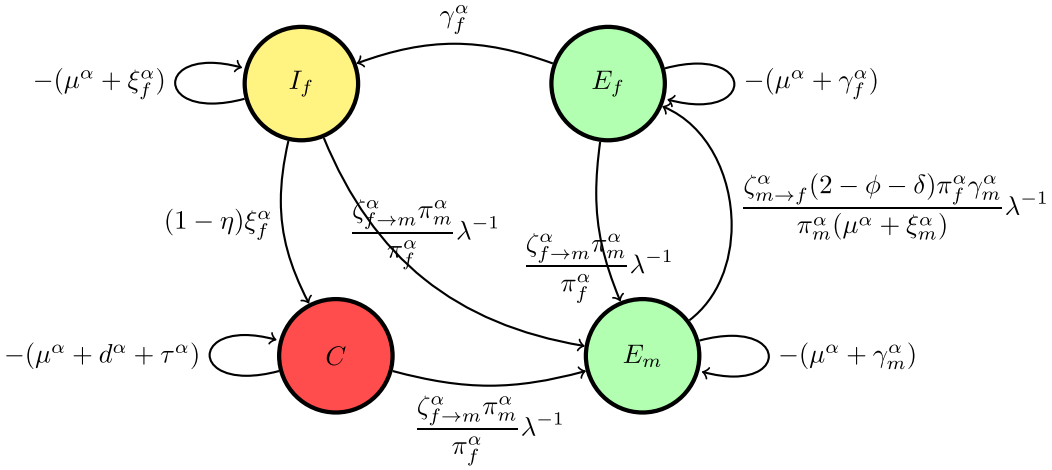


**Fig. 5.** (**B***) Digraph representation without node $I_m$.

The Gaussian algorithm for all other nodes in Figs. 7–8 is performed in the same manner as shown in Figs. 5 and 6 to yield the result Finally, from Theorem 3, setting the weight of the loop at node $E_f$ equal to zero gives the following polynomial equation for $\lambda$:

$$-(\mu^\alpha+\gamma_f^\alpha)+\frac{\zeta_{f\to m}^\alpha\zeta_{m\to f}^\alpha(2-\phi-\delta)\gamma_m^\alpha}{(\mu^\alpha+\xi_m^\alpha)(\mu^\alpha+\gamma_m^\alpha)}\left(1+\frac{(1-\eta)\xi_f^\alpha\gamma_f^\alpha}{(\mu^\alpha+\xi_f^\alpha)(\mu^\alpha+d^\alpha+\tau^\alpha)}\right)\lambda^{-2}=0 \tag{27}$$

The reciprocal of the smallest positive root, say $\lambda$ of the polynomial equation (27), gives the expression for $\mathcal{R}_e$.

$$\begin{aligned}\lambda^2&=\frac{\zeta_{f\to m}^\alpha\zeta_{m\to f}^\alpha(2-\phi-\delta)\gamma_m^\alpha}{(\mu^\alpha+\gamma_f^\alpha)(\mu^\alpha+\xi_m^\alpha)(\mu^\alpha+\gamma_m^\alpha)}\left(1+\frac{(1-\eta)\xi_f^\alpha\gamma_f^\alpha}{(\mu^\alpha+\xi_f^\alpha)(\mu^\alpha+d^\alpha+\tau^\alpha)}\right)\\ \Longrightarrow\ \mathcal{R}_e&=\sqrt{\frac{\zeta_{f\to m}^\alpha\zeta_{m\to f}^\alpha(2-\phi-\delta)\gamma_m^\alpha}{(\mu^\alpha+\gamma_f^\alpha)(\mu^\alpha+\xi_m^\alpha)(\mu^\alpha+\gamma_m^\alpha)}\left(1+\frac{(1-\eta)\xi_f^\alpha\gamma_f^\alpha}{(\mu^\alpha+\xi_f^\alpha)(\mu^\alpha+d^\alpha+\tau^\alpha)}\right)}\end{aligned} \tag{28}$$

### 2.4. Global stability at the Papillomavirus-Free Equilibrium

By applying a Lyapunov function within the Caputo derivative framework, we demonstrate that, even with the fractional dynamics of vaccination and treatment in the FSM (13), HPV can eventually be eradicated from the entire population.

**Theorem 4.** *For $\alpha\in(0,1)$, the matrix $Q$, which represents the HPV transmission dynamics, is irreducible. Therefore, the PFE of system (13) is globally asymptotically stable within the feasible region $\Omega$ when $\mathcal{R}_e\le 1$; otherwise, it becomes unstable.*

**Proof.** To establish the global stability of PFE that incorporates the Caputo derivative to account for the effects of memory and time delays in the system, we use a Goh-type Lyapunov function, typically expressed in the following form:

$$\mathcal{L}_0(t)=\sum_{i=1}^{n}b_i\left(x_i(t)-x_i^0-x_i^0\ln\frac{x_i(t)}{x_i^0}\right). \tag{29}$$

$$\begin{aligned}\mathcal{L}_0(t)&=b_1\left(S_f(t)-S_f^0-S_f^0\ln\frac{S_f(t)}{S_f^0}\right)+b_2\left(V(t)-V^0-V^0\ln\frac{V(t)}{V^0}\right)+b_3\left(E_f(t)-E_f^0-E_f^0\ln\frac{E_f(t)}{E_f^0}\right)\\&+b_4\left(I_f(t)-I_f^0-I_f^0\ln\frac{I_f(t)}{I_f^0}\right)+b_5\left(R_f(t)-R_f^0-R_f^0\ln\frac{R_f(t)}{R_f^0}\right)+b_6\left(C(t)-C^0-C^0\ln\frac{C(t)}{C^0}\right)\\&+b_7\left(S_m(t)-S_m^0-S_m^0\ln\frac{S_m(t)}{S_m^0}\right)+b_8\left(E_m(t)-E_m^0-E_m^0\ln\frac{E_m(t)}{E_m^0}\right)+b_9\left(I_m(t)-I_m^0-I_m^0\ln\frac{I_m(t)}{I_m^0}\right)\\&+b_{10}\left(R_m(t)-R_m^0-R_m^0\ln\frac{R_m(t)}{R_m^0}\right).\end{aligned}$$

Where $b_1,b_2,b_7$, are positive constants to be determined. Applying Definition 3–4 and Lemma 1.1 leads to:

$$\begin{aligned}{}_{t_0}^{C}D_t^\alpha\mathcal{L}_0(t)&\le b_1\left(1-\frac{S_f^0}{S_f(t)}\right){}_{t_0}^{C}D_t^\alpha S_f(t)+b_2\left(1-\frac{V^0}{V(t)}\right){}_{t_0}^{C}D_t^\alpha V(t)+b_7\left(1-\frac{S_m^0}{S_m(t)}\right){}_{t_0}^{C}D_t^\alpha S_m(t)\\&+b_3\left(1-\frac{E_f^0}{E_f(t)}\right){}_{t_0}^{C}D_t^\alpha E_f(t)+b_4\left(1-\frac{I_f^0}{I_f(t)}\right){}_{t_0}^{C}D_t^\alpha I_f(t)+b_5\left(1-\frac{R_f^0}{R_f(t)}\right){}_{t_0}^{C}D_t^\alpha R_f(t)\\&+b_6\left(1-\frac{C^0}{C(t)}\right){}_{t_0}^{C}D_t^\alpha C(t)+b_8\left(1-\frac{E_m^0}{E_m(t)}\right){}_{t_0}^{C}D_t^\alpha E_m(t)+b_9\left(1-\frac{I_m^0}{I_m(t)}\right){}_{t_0}^{C}D_t^\alpha I_m(t)\\&+b_{10}\left(1-\frac{R_m^0}{R_m(t)}\right){}_{t_0}^{C}D_t^\alpha R_m(t).\end{aligned} \tag{30}$$

By substituting the FSM (13) into Eq. (30), we observe that the constants $b_1=\dfrac{\mu^\alpha+\lambda_m^\alpha}{1-\phi}$, $b_2=\dfrac{\mu^\alpha+(1-\sigma)\lambda_f^\alpha}{\phi}$, and $b_7=\mu^\alpha+\lambda_m^\alpha$ are positive coefficients.

$$\begin{aligned}{}_{t_0}^{C}D_t^\alpha\mathcal{L}_0(t)&\le b_1\left(1-\frac{S_f^0}{S_f(t)}\right)((1-\phi)\pi_f^\alpha-(\mu^\alpha+\lambda_m)S_f(t))+b_2\left(1-\frac{V^0}{V(t)}\right)(\phi\pi_f^\alpha-\mu^\alpha V(t)-(1-\delta)\lambda_m V(t))\\&+b_7\left(1-\frac{S_m^0}{S_m(t)}\right)\pi_m^\alpha-(\mu^\alpha+\lambda_m)S_m(t)+b_3\left(1-\frac{E_f^0}{E_f(t)}\right)(\lambda_m S_f(t)+(1-\delta)\lambda_m V(t)-(\mu^\alpha+\gamma_f^\alpha)E_f(t))\\&+b_4\left(1-\frac{I_f^0}{I_f(t)}\right)(\gamma_f^\alpha E_f(t)-(\mu^\alpha+\eta)I_f(t))+b_5\left(1-\frac{R_f^0}{R_f(t)}\right)(\eta I_f(t)+\tau^\alpha C(t)-\mu^\alpha R_f(t))\\&+b_6\left(1-\frac{C^0}{C(t)}\right)((1-\eta)I_f(t)-(\mu^\alpha+d^\alpha+\tau^\alpha)C(t))+b_8\left(1-\frac{E_m^0}{E_m(t)}\right)(\lambda_f S_m(t)-(\mu^\alpha+\gamma_m^\alpha)E_m(t))\\&+b_9\left(1-\frac{I_m^0}{I_m(t)}\right)(\gamma_m^\alpha E_m(t)-(\mu^\alpha+\xi^\alpha)I_m(t))+b_{10}\left(1-\frac{R_m^0}{R_m(t)}\right)(\xi^\alpha I_m(t)-\mu^\alpha R_m(t))\end{aligned}$$

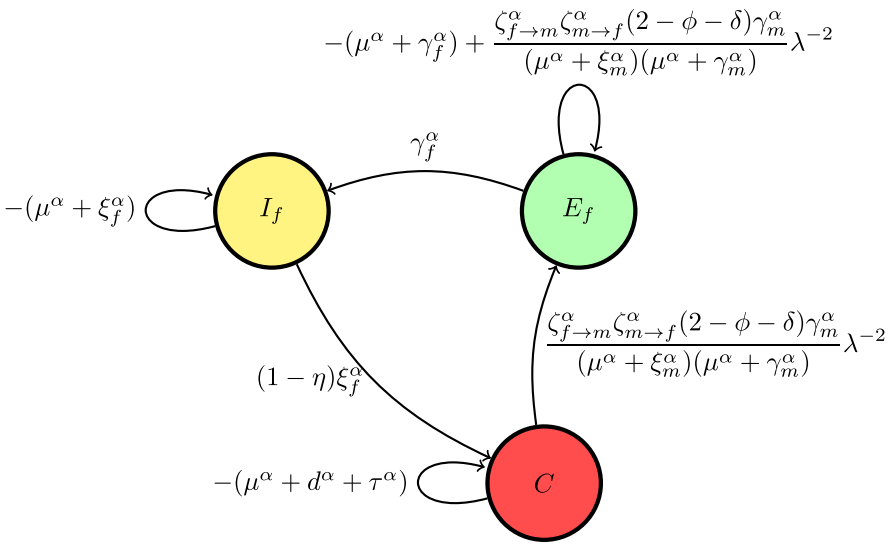


**Fig. 6.** (C*) Digraph representation without node $E_m$.

Through algebraic manipulations and simplification, the model assumes no memory effects in the infectious class within the population, as the Caputo fractional derivative reveals that as $\alpha \to 1$. Consequently, the analysis focuses exclusively on the susceptible and vaccinated individuals.

$$\begin{aligned}
{}_{t_0}^{C}D_t^\alpha \mathcal{L}_0(t) \le & -\left(\frac{\mu^\alpha+\lambda_m^\alpha}{1-\phi}\right)\frac{(S_f(t)-S_f^0)^2}{S_f(t)} - \left(\frac{\mu^\alpha+(1-\delta)\lambda_m^\alpha}{\phi}\right)\frac{(V(t)-V^0)^2}{V(t)} - (\mu^\alpha+\lambda_f)\frac{(S_m(t)-S_m^0)^2}{S_m(t)} \\
& - \frac{\zeta_{f\to m}^\alpha\zeta_{m\to f}^\alpha\gamma_m^\alpha}{(\mu^\alpha+\gamma_f^\alpha)(\mu^\alpha+\gamma_m^\alpha)}\left\{\frac{(E_m(t)-E_m^0)^2}{E_m(t)}+\frac{(E_f(t)-E_f^0)^2}{E_f(t)}\right\} \\
& - \frac{(1-\eta)\zeta_{f\to m}^\alpha\zeta_{m\to f}^\alpha(2-\phi-\delta)\gamma_m^\alpha\gamma_f^\alpha}{(\mu^\alpha+d^\alpha+\tau^\alpha)(\mu^\alpha+\gamma_f^\alpha)(\mu^\alpha+\xi_m^\alpha)}\left\{\frac{(R_f(t)-R_f^0)^2}{R_f(t)}+\frac{(C(t)-C^0)^2}{C(t)}+\frac{(I_f(t)-I_f^0)^2}{I_f(t)}\right\} \\
& - \frac{(1-\eta)\zeta_{f\to m}^\alpha\zeta_{m\to f}^\alpha\gamma_m^\alpha\gamma_f^\alpha}{(\mu^\alpha+\xi_f^\alpha)(\mu^\alpha+\gamma_f^\alpha)(\mu^\alpha+\gamma_m^\alpha)}\left\{\frac{(I_m(t)-I_m^0)^2}{I_m(t)}+\frac{(R_m(t)-R_m^0)^2}{R_m(t)}\right\}.
\end{aligned} \tag{31}$$

It follows that

$$\begin{aligned}
{}_{t_0}^{C}D_t^\alpha \mathcal{L}_0(t) \le & -\left\{\left(\frac{\mu^\alpha+\lambda_m^\alpha}{1-\phi}\right)\frac{(S_f(t)-S_f^0)^2}{S_f(t)} + \left(\frac{\mu^\alpha+(1-\delta)\lambda_m^\alpha}{\phi}\right)\frac{(V(t)-V^0)^2}{V(t)} + (\mu^\alpha+\lambda_f^\alpha)\frac{(S_m(t)-S_m^0)^2}{S_m(t)}\right\} \\
& - \frac{\zeta_{f\to m}^\alpha\zeta_{m\to f}^\alpha\gamma_m^\alpha}{(\mu^\alpha+\gamma_f^\alpha)(\mu^\alpha+\gamma_m^\alpha)}\Psi_1 - \frac{(1-\eta)\zeta_{f\to m}^\alpha\zeta_{m\to f}^\alpha(2-\phi-\delta)\gamma_m^\alpha\gamma_f^\alpha}{(\mu^\alpha+d^\alpha+\tau^\alpha)(\mu^\alpha+\gamma_f^\alpha)(\mu^\alpha+\xi_m^\alpha)}\Psi_2 - \frac{(1-\eta)\zeta_{f\to m}^\alpha\zeta_{m\to f}^\alpha\gamma_m^\alpha\gamma_f^\alpha}{(\mu^\alpha+\xi_f^\alpha)(\mu^\alpha+\gamma_f^\alpha)(\mu^\alpha+\gamma_m^\alpha)}\Psi_3 \\
& - \frac{\zeta_{f\to m}^\alpha\zeta_{m\to f}^\alpha(2-\phi-\delta)(1-\eta)\xi_f^\alpha\gamma_f^\alpha\gamma_m^\alpha}{(\mu^\alpha+\gamma_f^\alpha)(\mu^\alpha+\xi_m^\alpha)(\mu^\alpha+\gamma_m^\alpha)(\mu^\alpha+d^\alpha+\tau^\alpha)}(1-\mathcal{R}_e^2).
\end{aligned} \tag{32}$$

The digraph $\mathcal{G}(\mathbf{A}^*)$ is strongly connected, indicating that all compartments (vertices) in the epidemiological model are interlinked through directed pathways, ensuring that even non-interacting states are ultimately connected by a transmission route. Furthermore, the matrix $Q$ is non-negative and irreducible, signifying that all potential transitions between compartments are possible, with no isolated subgroups or disconnected segments within the system. According to the Perron–Frobenius theorem [47], since all parameters and variables in system (13) are nonnegative, it follows that ${}_{t_0}^{C}D_t^\alpha \mathcal{L}_0(t) < 0$, which guarantees that the effective reproduction number $\mathcal{R}_e \le 1$.

Moreover, the LaSalle invariance principle [48] demonstrates that PFE of system (13) is globally asymptotically stable when $\mathcal{R}_e < 1$, meaning that HPV infections will eventually be eradicated from the population. This finding underscores the importance of sustained public health interventions, including vaccination and treatment strategies, in controlling HPV transmission and reducing the incidence of related conditions, such as cervical cancer. □

### 2.5. Global stability of the endemic state

We establish that the endemic equilibrium $E^* = (S_f^*, V^*, E_f^*, I_f^*, R_f^*, C^*, S_m^*, E_m^*, I_m^*, R_m^*)$ is globally asymptotically stable within the biologically meaningful region $\Omega^0$, provided the effective reproduction number satisfies $\mathcal{R}_e > 1$. This equilibrium resides in the interior of the feasible space $\Omega^0$, where all state variables retain positive, epidemiologically valid values.

According to the uniform persistence framework outlined in [49] and extended in Proposition 3.3 of [50], when the disease-free equilibrium $E_0$ becomes unstable, the system described by FSM (13) exhibits uniform persistence within $\Omega^0$. Moreover, solution trajectories remain bounded in this region, as demonstrated by inequality (14), ensuring the long-term persistence of the infection.

The coexistence of bounded solutions and uniform persistence implies the presence of an endemic equilibrium $E^*$ within the interior $\Omega^0$, confirming the long-term survival of the disease when $\mathcal{R}_e > 1$ [51]. From a biological standpoint, this reflects the tendency of the infection to establish a stable presence in the population when transmission outpaces recovery and control.

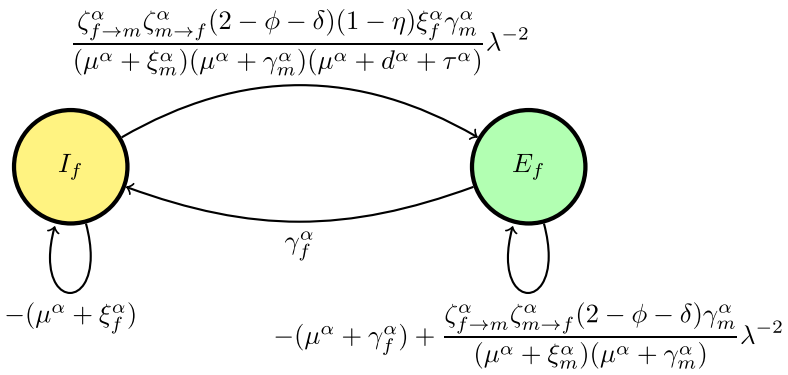


**Fig. 7.** (**D***) Digraph representation without node $C$.

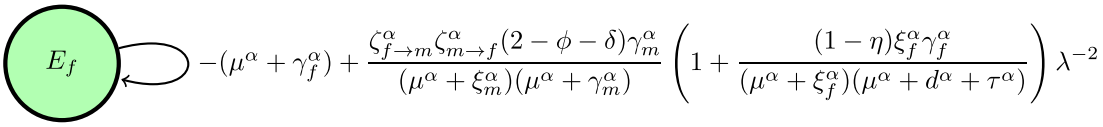


**Fig. 8.** (**E**) Digraph representation without node $I_f$.

The global stability of $E^*$ is supported by the structural properties of the system's Jacobian. The following lemma, adapted from [52], provides the foundational linear algebraic result needed:

**Lemma 2.1.** *Let $Q_{5\times5}$ be an irreducible matrix. Then the homogeneous linear system*

$$Qu = 0 \tag{33}$$

*possesses the following properties:*

- *The solution space within $\Omega^0$ is one-dimensional.*
- *A basis vector is given by $u = (u_1, u_2, \dots, u_5)$ where each $u_k$ corresponds to the $k$th diagonal entry of $Q$, for $1 \le k \le 5$.*

**Theorem 5.** *If the digraph corresponding to $Q$ is strongly connected and $\mathcal{R}_e > 1$, then the endemic equilibrium of FSM (13) is globally asymptotically stable in the feasible region $\Omega^0$.*

**Proof.** To verify the global stability of the endemic state $E^*$, we use the fact that the irreducibility of $Q$ ensures the positivity of all components $u_k$ in the domain $\Omega^0$, which implies irreducibility of FSM (13). We construct a Lyapunov function, inspired by the Goh–Volterra framework [26,53–55], that aggregates contributions from each epidemiological class. This function $\mathcal{L} : \Omega^0 \to \mathbb{R}_+$ is designed to demonstrate that deviations from $E^*$ diminish over time, confirming the global asymptotic stability of the endemic equilibrium.

$$\mathcal{L}(t) = \sum_{i=1}^{n} c_i \left( x_i(t) - x_i^* - x_i^* \ln \frac{x_i(t)}{x_i^*} \right). \tag{34}$$

$$\begin{aligned}
\mathcal{L}(t) = {} & c_1 \left( S_f(t) - S_f^* - S_f^* \ln \frac{S_f(t)}{S_f^*} \right) + c_2 \left( V(t) - V^* - V^* \ln \frac{V(t)}{V^*} \right) + c_3 \left( E_f(t) - E_f^* - E_f^* \ln \frac{E_f(t)}{E_f^*} \right) \\
& + c_4 \left( I_f(t) - I_f^* - I_f^* \ln \frac{I_f(t)}{I_f^*} \right) + c_5 \left( R_f(t) - R_f^* - R_f^* \ln \frac{R_f(t)}{R_f^*} \right) + c_6 \left( C - C^* - C^* \ln \frac{C}{C^*} \right) \\
& + c_7 \left( S_m(t) - S_m^* - S_m^* \ln \frac{S_m(t)}{S_m^*} \right) + c_8 \left( E_m(t) - E_m^* - E_m^* \ln \frac{E_m(t)}{E_m^*} \right) + c_9 \left( I_m(t) - I_m^* - I_m^* \ln \frac{I_m(t)}{I_m^*} \right) \\
& + c_{10} \left( R_m(t) - R_m^* - R_m^* \ln \frac{R_m(t)}{R_m^*} \right).
\end{aligned}$$

Let $c_i$, where $i = 1, 2, 3, \dots, 10$, be positive constants to be determined. Applying Definition 3–4 and Lemma 1.1 leads to:

$$\begin{aligned}
{}_{t_0}^{C}D_t^\alpha \mathcal{L}(t) \le {} & c_1 \left( 1 - \frac{S_f^*}{S_f(t)} \right) {}_{t_0}^{C}D_t^\alpha S_f(t) + c_2 \left( 1 - \frac{V^*}{V(t)} \right) {}_{t_0}^{C}D_t^\alpha V(t) + c_3 \left( 1 - \frac{E_f^*}{E_f(t)} \right) {}_{t_0}^{C}D_t^\alpha E_f(t) \\
& + c_4 \left( 1 - \frac{I_f^*}{I_f(t)} \right) {}_{t_0}^{C}D_t^\alpha I_f(t) + c_5 \left( 1 - \frac{R_f^*}{R_f(t)} \right) {}_{t_0}^{C}D_t^\alpha R_f(t) + c_6 \left( 1 - \frac{C^*}{C(t)} \right) {}_{t_0}^{C}D_t^\alpha C(t) \\
& + c_7 \left( 1 - \frac{S_m^*}{S_m(t)} \right) {}_{t_0}^{C}D_t^\alpha S_m(t) + c_8 \left( 1 - \frac{E_m^*}{E_m(t)} \right) {}_{t_0}^{C}D_t^\alpha E_m(t) + c_9 \left( 1 - \frac{I_m^*}{I_m(t)} \right) {}_{t_0}^{C}D_t^\alpha I_m(t) \\
& + c_{10} \left( 1 - \frac{R_m^*}{R_m(t)} \right) {}_{t_0}^{C}D_t^\alpha R_m(t),
\end{aligned} \tag{35}$$

with a condition that $\Phi(x) = 1 - x + \ln x \leq 0 : \Phi(x) = 0 \iff x = 1$.

By substituting the FSM (13) into Eq. (35), we observe that

$$\begin{aligned}
{}_{t_0}^{C}D_t^{\alpha}\mathcal{L}(t) \leq\ & c_1\left(1-\frac{S_f^*}{S_f(t)}\right)((1-\phi)\pi_f^{\alpha}-(\mu^{\alpha}+\lambda_m^{\alpha})S_f(t))+c_2\left(1-\frac{V^*}{V(t)}\right)(\phi\pi_f^{\alpha}-\mu^{\alpha}V(t)-(1-\delta)\lambda_m^{\alpha}V(t))\\
&+c_3\left(1-\frac{E_f^*}{E_f(t)}\right)(\lambda_m^{\alpha}S_f(t)+(1-\delta)\lambda_m^{\alpha}V(t)-(\mu^{\alpha}+\gamma_f^{\alpha})E_f(t))\\
&+c_4\left(1-\frac{I_f^*}{I_f(t)}\right)(\gamma_f^{\alpha}E_f(t)-(\mu^{\alpha}+\xi_f^{\alpha})I_f(t))+c_5\left(1-\frac{R_f^*}{R_f(t)}\right)(\eta\xi_f^{\alpha}I_f(t)+\tau^{\alpha}C(t)-\mu^{\alpha}R_f(t))\\
&+c_6\left(1-\frac{C^*}{C(t)}\right)((1-\eta)\xi_f^{\alpha}I_f(t)-(\mu^{\alpha}+d^{\alpha}+\tau^{\alpha})C(t))+c_7\left(1-\frac{S_m^*}{S_m(t)}\right)\pi_m^{\alpha}-(\mu^{\alpha}+\lambda_f^{\alpha})S_m(t)\\
&+b_8\left(1-\frac{E_m^*}{E_m(t)}\right)(\lambda_f^{\alpha}S_m(t)-(\mu^{\alpha}+\gamma_m^{\alpha})E_m(t))+c_9\left(1-\frac{I_m^*}{I_m(t)}\right)(\gamma_m^{\alpha}E_m(t)-(\mu^{\alpha}+\xi_m^{\alpha})I_m(t))\\
&+c_{10}\left(1-\frac{R_m^*}{R_m(t)}\right)(\xi_m^{\alpha}I_m(t)-\mu^{\alpha}R_m(t))
\end{aligned} \tag{36}$$

Utilizing the following identities which exists at the endemic point

$$\begin{cases}
(1-\phi)\pi_f^{\alpha} &= (\mu^{\alpha}+\lambda_m^*)S_f^*, \qquad \phi\pi_f^{\alpha}=\mu^{\alpha}V^*+(1-\delta)\lambda_m^*V^*,\\
\lambda_m S_f^* &= -(1-\delta)\lambda_m^*V^*+(\mu^{\alpha}+\gamma_f^{\alpha})E_f^*, \qquad \xi_m^{\alpha}I_m^*=\mu^{\alpha}R_m^*,\\
\gamma_f^{\alpha}E_f^* &= (\mu^{\alpha}+\xi_f^{\alpha})I_f^*, \qquad \eta\xi_f^{\alpha}I_f^*=-\tau^{\alpha}C^*+\mu^{\alpha}R_f^*\\
(1-\eta)\xi_f^{\alpha}I_f^* &= (\mu^{\alpha}+d^{\alpha}+\tau^{\alpha})C(t), \qquad \pi_m^{\alpha}=(\mu^{\alpha}-\lambda_m)S_m^*,\\
\lambda_m S_m^* &= -(\mu^{\alpha}+\gamma_m^{\alpha})E_m^*, \qquad \gamma_m^{\alpha}E_m^*=(\mu^{\alpha}+\xi_m^{\alpha})I_m^*
\end{cases} \tag{37}$$

Substituting identities (37) into (36) and simplifying, one gets

$$\begin{aligned}
{}_{t_0}^{C}D_t^{\alpha}\mathcal{L}(t) \leq\ & .(\mu^{\alpha}+\lambda_m^{\alpha*})S_f^*\underbrace{\left(2-\frac{S_f(t)}{S_f^*}-\frac{S_f^*}{S_f(t)}\right)}_{(1)}+(1-\delta)\lambda_f^{\alpha*}V^*S_m^*\underbrace{\left(2-\frac{V^*}{V(t)}-\frac{E_f(t)}{E_f^*}-\frac{S_m(t)V^*I_f(t)}{S_m^*V(t)I_f^*}+\frac{I_m(t)}{I_m^*}\right)}_{(2)}\\
&+(\mu^{\alpha}+\gamma_f^{\alpha})(\mu^{\alpha}+d^{\alpha}+\tau^{\alpha})C^*S_f^*\underbrace{\left(4-\frac{S_m^*}{S_m}-\frac{R_f^*}{R_f(t)}-\frac{I_f(t)}{I_f^*}-\frac{S_f(t)I_m^*C(t)}{S_f^*I_m(t)C^*}-\frac{S_m(t)C^*I_m(t)}{S_m^*C(t)I_m^*}\right)}_{(3)}\\
&+\left(\frac{(1-\delta)\lambda_m^{\alpha*}(\mu^{\alpha}+\lambda_f^{\alpha*})}{(\mu^{\alpha}+\gamma_m^{\alpha})(\mu^{\alpha}+d^{\alpha}+\tau^{\alpha})}\right)\underbrace{\left(2-\frac{V(t)}{V^*}-\frac{V^*}{V(t)}\right)\left(4-\frac{S_m(t)}{S_m^*}-\frac{S_m^*}{S_m(t)}-\frac{C^*}{C(t)}-\frac{E_m(t)}{E_m^*}\right)}_{(4)}\\
&+(\mu^{\alpha}+\xi_f^{\alpha})(\mu^{\alpha}+\xi_m^{\alpha})I_m^*E_f^*\underbrace{\left(2-\frac{C^*}{C(t)}-\frac{E_m(t)}{E_m^*}-\frac{R_m(t)V^*I_m(t)}{R_m^*V(t)I_m^*}+\frac{R_f(t)}{R_f^*}\right)}_{(5)}\\
&+(\mu^{\alpha}+\lambda_f^{\alpha*})S_m^*\underbrace{\left(2-\frac{S_m(t)}{S_m^*}-\frac{S_m^*}{S_m(t)}\right)}_{(6)}+(1-\delta)\lambda_m^{\alpha*}R_m^*S_f^*\underbrace{\left(2-\frac{C^*}{C(t)}-\frac{E_f(t)}{E_f^*}-\frac{R_f(t)V^*I_m(t)}{R_f^*V(t)I_m^*}+\frac{I_f(t)}{I_f^*}\right)}_{(7)}\\
&+(\mu^{\alpha}+\xi_f^{\alpha})(\mu^{\alpha}+\xi_m^{\alpha})I_m^*E_f^*\underbrace{\left(2-\frac{C^*}{C(t)}-\frac{E_m(t)}{E_m^*}-\frac{R_m(t)V^*I_m(t)}{R_m^*V(t)I_m^*}+\frac{R_f(t)}{R_f^*}\right)}_{(8)}\\
&+\frac{(\mu^{\alpha}+\lambda_m^{\alpha*})(\mu^{\alpha}+\lambda_f^{\alpha*})}{(\mu^{\alpha}+\gamma_f^{\alpha})(\mu^{\alpha}+d^{\alpha}+\tau^{\alpha})}S_m^*S_f^*\underbrace{\left(2-\frac{R_m(t)}{R_m^*}-\frac{R_m^*}{R_m(t)}\right)\left(2-\frac{R_f(t)}{R_f^*}-\frac{R_f^*}{R_f(t)}-\frac{S_m(t)C^*I_m(t)}{S_m^*C(t)I_m^*}+\frac{V(t)}{V^*}\right)}_{(9)}\\
&+(1-\delta)\lambda_m^*\alpha*R_m^*S_f^*\underbrace{\left(2-\frac{I_f^*}{I_f(t)}-\frac{E_m(t)}{E_m^*}-\frac{R_f(t)V^*I_m(t)}{R_f^*V(t)I_m^*}+\frac{C(t)}{C^*}\right)}_{(10)}.
\end{aligned} \tag{38}$$

Since the arithmetic mean is greater than or equal to the geometric mean, it follows that for (1), (4) and (6) from (38), the following is satisfied: $\left(2-\frac{S_f^*}{S_f(t)}-\frac{S_f(t)}{S_f^*}\right)\leq 0$, $\left(2-\frac{S_m^*}{S_m(t)}-\frac{S_m(t)}{S_m^*}\right)\leq 0$, and $\left(2-\frac{V(t)}{V^*}-\frac{V^*}{V(t)}\right)\left(4-\frac{S_m(t)}{S_m^*}-\frac{S_m^*}{S_m(t)}-\frac{C^*}{C(t)}-\frac{E_m(t)}{E_m^*}\right)\leq 0$.

Consider the condition $\Phi(x) = 1 - x + \ln(x)$ for $x > 0$. It follows that $\Phi(x) \leq 0$, with equality only when $x = 1$. Using the properties of $\Phi(x)$, we can show that the terms for (2), (3), (5), (7), (8), (9), and (10) are less than or equal to zero. As a result, $\mathcal{L}(S_f, V, E_f, I_f, R_f, C, S_m, E_m, I_m, R_m)$

**Table 2**
Descriptions and values of model parameters with their respective sources.

| Parameter | Biological/Epidemiological Description | Value | Source |
|---|---|---|---|
| $\pi_f^\alpha$, $\pi_m^\alpha$ | Entry rate of sexually active females and males into the population. | 999 300 | [9,56] |
| $\delta$ | Effectiveness of the HPV vaccine in preventing infection. | 0.45 | Fitted |
| $\phi$ | Proportion of incoming sexually active females who are vaccinated. | 0.4214 | Fitted |
| $\tau^\alpha$ | Rate at which cervical cancer patients receive treatment. | 0.25 | Fitted |
| $\xi_m^\alpha$, $\xi_f^\alpha$ | Recovery or progression rate from the infectious stage for males and females. | 0.769, 0.211 | [10], Fitted |
| $\eta$, $1-\eta$ | Fraction of infected females who recover vs. progress to cervical cancer. | 0.36, 0.64 | Fitted |
| $\psi_f$, $\psi_m$ | Adjustment factor reflecting reduced infectiousness of exposed individuals. | 0.85, 0.43 | [57] |
| $\mu^\alpha$ | Baseline (natural) mortality rate. | 0.015 | [9,56] |
| $d^\alpha$ | Mortality rate due to cervical cancer. | 0.162 | Fitted |
| $\zeta_{f\to m}^\alpha$, $\zeta_{m\to f}^\alpha$ | Probability of HPV transmission per contact from female to male and vice versa. | 0.51, 0.51 | Fitted, [58] |
| $\gamma_f^\alpha$, $\gamma_m^\alpha$ | Transition rate from exposed to symptomatic infection in females and males. | 0.461, 0.0157 | Fitted, [58] |

serves as a Lyapunov function on $\Omega^0$, and $E^0$ is the largest invariant set where ${}_{t_0}^{C}D_t^\alpha \mathcal{L}(t) = 0$. By LaSalle's invariance principle [48], $E^0$ is globally stable in $\Omega^0$.

Epidemiologically, if $\mathcal{R}_e$ exceeds unity, HPV infections will spread within the population, increasing the risk of cervical cancer and related mortality. However, with the implementation of vaccination and treatment strategies, the spread of HPV can be controlled. Without such interventions, HPV infections will persist, leading to a continued rise in the burden of cervical cancer and associated deaths. □

### 2.6. Parameter estimation of the model using Markov chain Monte Carlo (MCMC)

To obtain numerical results for FSM (13), it is necessary to estimate its parameters. We derive these parameter values using two methods: certain parameters are taken from existing literature, while others are estimated by minimizing the root-mean square error (RMSE), computed as follows:

$$\text{RMSE} = \sqrt{\frac{1}{n}\sum_{i=1}^{n}(\text{Estimate} - \text{Synthetic})^2}, \tag{39}$$

where $n$ denotes the total number of synthetic data points, the annual incidence of infection and disease progression is captured by the fourth and sixth terms, respectively. Specifically, the expressions ${}_{t_0}^{C}D_t^\alpha I_f(t)$ and ${}_{t_0}^{C}D_t^\alpha C(t)$ represent the estimated number of new infections and annual cervical cancer cases, serving as proxies for infection incidence and cancer incidence within the population modeled in FSM (13). These model outputs are critical for calibrating the force of infection and cancer burden over time. The corresponding parameter values used in the dynamic transmission model are summarized in Table 2. For the initial conditions of the population compartments, we adopt estimates grounded in demographic and epidemiological data, as informed by the studies of [1,9,56].

$S_f(0) = 5365499$, $V(0) = 600000$, $E_f(0) = 100000$, $I_f(0) = 60000$, $R_f(0) = 20$, $C(0) = 10868$, $S_m(0) = 5365499$, $E_m(0) = 1000$, $I_m(0) = 60$, $R_m(0) = 0$.

To estimate the transition rates between epidemiological compartments, we used Markov Chain Monte Carlo (MCMC) methods to calibrate the parameters of interest (listed in Table 2), ensuring consistency with the simulated data. These parameters govern critical processes such as vaccination uptake, infection clearance, disease progression, and mortality.

Fig. 9 presents pairwise scatter plots illustrating the relationship between key epidemiological parameters and the effective reproduction number ($\mathcal{R}e$), using posterior samples derived from a Bayesian framework. Each subplot demonstrates how variations in parameters, such as female-to-male transmission modifiers ($\zeta_{f\to m}^\alpha$), progression rates ($\gamma_f^\alpha$), and the rate at which infected females progress to cervical cancer, are positively correlated with $\mathcal{R}_e$. Specifically, increases in these parameters lead to an increase in $\mathcal{R}_e$. Conversely, disease-induced mortality ($d^\alpha$), the treatment rate for females who have developed cervical cancer, and other parameters shown in Fig. 9 are negatively correlated with $\mathcal{R}_e$; that is, increases in these parameters result in a decrease in $\mathcal{R}_e$, signifying a reduction in HPV infections and cervical cancer cases. The blue stars represent the maximum a posteriori (MAP) estimates. The scatter plots reveal the sensitivity of $\mathcal{R}_e$ to changes in these parameters, offering insight into the most influential factors driving transmission dynamics.

We analyze the impact of individual parameters on the effective reproduction number ($\mathcal{R}_e$) by simultaneously varying all model inputs and employing the Partial Rank Correlation Coefficient (PRCC) method, as described in [59,60]. The results, presented in Fig. 10, show that higher female recruitment rates, increased contact rates between sexually active males and females, and elevated transmission coefficients significantly contribute to the spread of the disease. In contrast, the simulations indicate that improved treatment rates, higher vaccination coverage among females, natural recovery, and greater vaccine efficacy are all strongly associated with a reduction in transmission potential. These findings emphasize the importance of implementing public health interventions such as vaccination programs and awareness campaigns to effectively lower transmission rates. Moreover, the analysis identifies natural recovery as the most influential factor in reducing the transmission potential of cervical cancer incidences.

### 2.7. Hyers–Ulam stability of fractional Caputo derivative for HPV

In this part, we establish the global stability to ensures that small perturbations in the FSM (13), such as changes in vaccination or treatment rates, will not lead to drastic changes in the long-term behavior of the epidemic model.

$${}_{t_0}^{C}D_t^\alpha v(t) = \Omega(t, v(t)), \quad t \geq 0, \quad v(0) = v_0 \in \mathbb{R}^+, \quad \text{where} \quad \Omega : \mathbb{R}^+ \times \mathbb{R}^{10} \to \mathbb{R}, \tag{40}$$

Consider the inequality

$$\|{}_{t_0}^{C}D_t^\alpha v(t) - \Omega(t, v(t))\|_1 < \epsilon, \quad \forall t \in [0, T]. \tag{41}$$

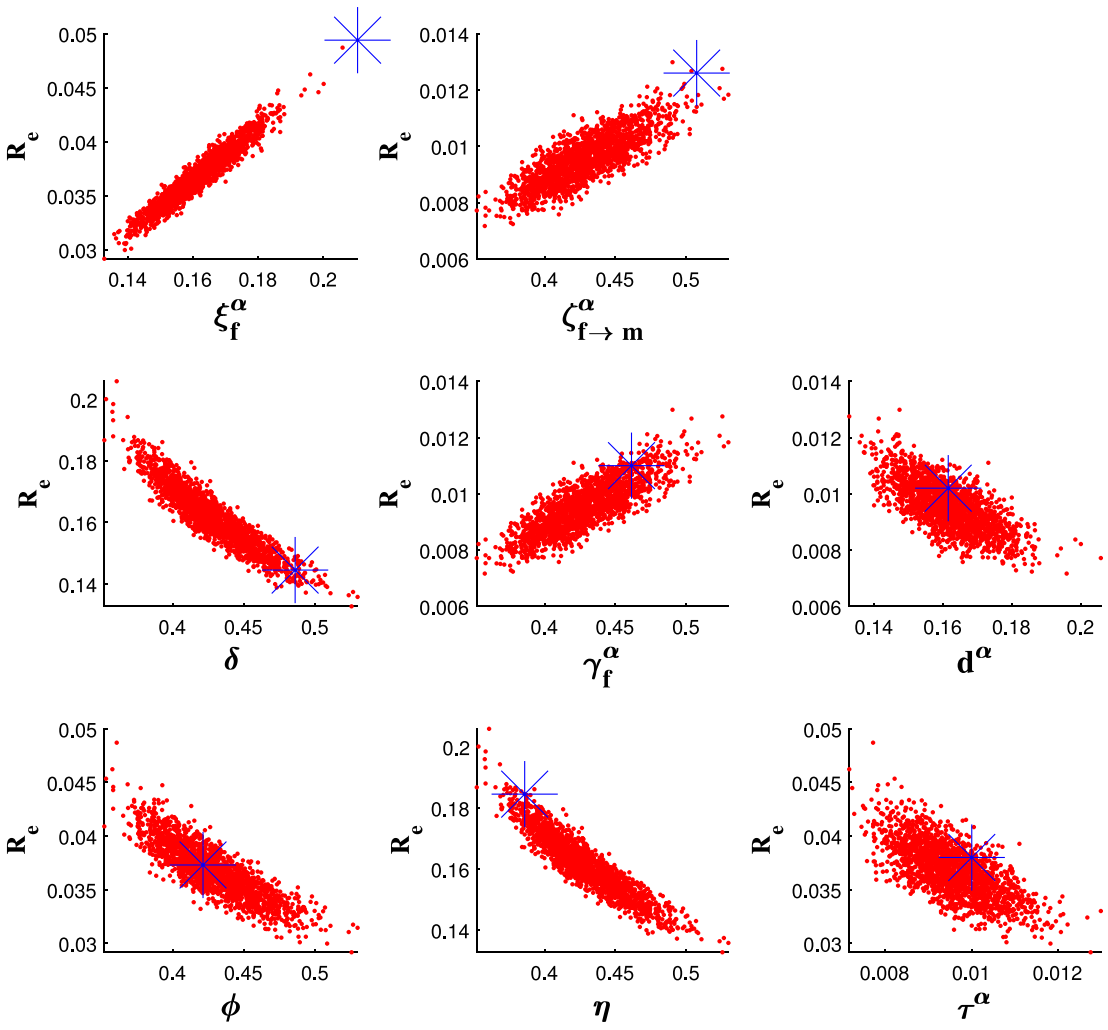


**Fig. 9.** Pairwise scatter plots showing how parameters relate to $\mathcal{R}_e$, with blue stars marking estimates.

**Lemma 2.2.** *Suppose $\Omega(t, v(t))$ holds for the following conditions:*

- *$\Omega$ is a continuous function with respect to $t$ for every $v(t) \in \mathbb{R}^n$,*
- *$\Omega$ and $\frac{\partial \Omega}{\partial v}$ are continuous functions with respect to $v(t) \in \mathbb{R}^n$.*

**Definition 9.** Now, $z \in \mathbb{E}$ is a solution of Eq. (40) if and only if there exists an $\vartheta \in \mathbb{E}$ such that:

$$|\vartheta(t)| \leq \varrho, \quad \text{where} \quad \vartheta = \max(\vartheta_j)^T, \quad j = 1, \ldots, 10, \text{and} \quad {}^{C}_{t_0}D^{\alpha}_{t} z(t) = \Omega(t, z(t)) + \vartheta(t), \quad \forall t \in [0, T], \tag{42}$$

Using the definition 1 and applying the fractional R-LF integral to (42) results in:

$$z(t) = z_0 + \frac{1}{\Gamma(\alpha)} \int_0^t (t-\varsigma)^{\alpha-1} \Omega(\varsigma, z(\varsigma))\, d\varsigma + \frac{1}{\Gamma(\alpha)} \int_0^t (t-\varsigma)^{\alpha-1} \vartheta(\varsigma)\, d\varsigma. \tag{43}$$

Consider the expression

$$\left\| z(t) - z_0 - \frac{1}{\Gamma(\alpha)} \int_0^t (t-\varsigma)^{\alpha-1} \Omega(\varsigma, z(\varsigma))\, d\varsigma \right\|_1. \tag{44}$$

Substitute the expression for $z(t)$ from (43) into (44) and applying condition (42) gives

$$\begin{aligned} \left\| z(t) - z_0 - \frac{1}{\Gamma(\alpha)} \int_0^t (t-\varsigma)^{\alpha-1} \Omega(\varsigma, z(\varsigma))\, d\varsigma \right\|_1 &= \left| \frac{1}{\Gamma(\alpha)} \int_0^t (t-\tau)^{\alpha-1} \vartheta(\varsigma)\, d\tau \right|. \\ &\leq \frac{1}{\Gamma(\alpha)} \int_0^t (t-\varsigma)^{\alpha-1} |\vartheta(\varsigma)|\, d\varsigma \\ &\leq \frac{\varrho}{\Gamma(\alpha)} \int_0^t (t-\varsigma)^{\alpha-1}\, d\varsigma \\ &\leq \frac{\varrho T^{\alpha}}{\Gamma(\alpha+1)} \end{aligned} \tag{45}$$

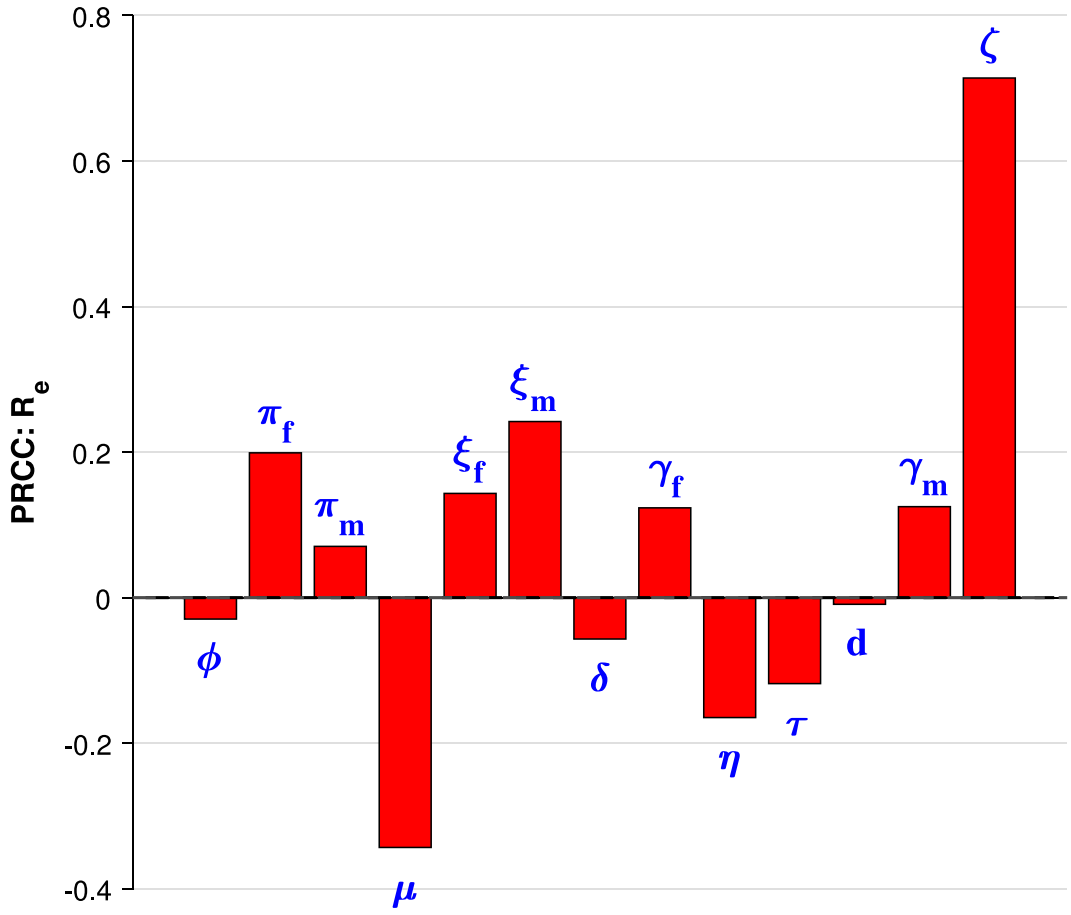


**Fig. 10.** Sensitivity analysis of $\mathcal{R}_e$ with respect to its model parameters.

Therefore

$$\left\| z(t) - z_0 - \frac{1}{\Gamma(\alpha)} \int_0^t (t-\varsigma)^{\alpha-1} \Omega(\varsigma, z(\varsigma))\, d\varsigma \right\|_1 \leq \frac{\varrho T^\alpha}{\Gamma(\alpha+1)}, \quad \forall t \in [0,T] \tag{46}$$

**Definition 10.** The fractional-order HPV model (13) is said to be Hyers–Ulam stable on the interval $[0,T]$ if there exists a constant $\chi > 0$ such that for every $\varrho > 0$ and a solution $z \in \mathbb{E}$ satisfying (44), a unique solution $v \in \mathbb{E}$ to (40) exists, with $\|z(t) - v(t)\|_1 < \chi\varrho, \quad \forall t \in [0,T], \quad$ where $\chi = \max(\chi_j)^T$.

**Theorem 6.** *Suppose that (40) and (44) together with definition 9 hold. Then, the HPV fractional model (13) is Hyers–Ulam stable on* $[0,T]$ *if* $\Gamma(\alpha+1) > \eta T^\alpha$ *hold*

**Proof.** By using definition 1 and Lemma 2.2, we can get that

$$v(t) = v_0 + \frac{1}{\Gamma(\alpha)} \int_0^t (t-\varsigma)^{\alpha-1} \Omega(\tau, v(\varsigma))\, d\varsigma. \tag{47}$$

Now, suppose $y_0 = v_0$ using Eqs. (46) and (47), we compute $\|y(t) - v(t)\|_1$ as follows:

$$\|z(t) - v(t)\|_1 = \left\| z(t) - z_0 - \frac{1}{\Gamma(\alpha)} \int_0^t (t-\varsigma)^{\alpha-1} \Omega(\varsigma, v(\varsigma))\, d\varsigma \right\|_1 \tag{48}$$

By adding and subtracting the term $\frac{1}{\Gamma(\alpha)} \int_0^t (t-\varsigma)^{\alpha-1} \Omega(\varsigma, z(\varsigma))\, d\varsigma$ on (48) and applying the triangle inequality, we have

$$\|z(t) - v(t)\|_1 \leq \varpi + \left| \frac{1}{\Gamma(\alpha)} \int_0^t (t-\varsigma)^{\alpha-1} \Omega(\varsigma, z(\varsigma))\, d\varsigma - \frac{1}{\Gamma(\alpha)} \int_0^t (t-\varsigma)^{\alpha-1} \Omega(\varsigma, v(\varsigma))\, d\varsigma \right| \tag{49}$$

where by $\varpi = \left\| z(t) - z_0 - \frac{1}{\Gamma(\alpha)} \int_0^t (t-\varsigma)^{\alpha-1} \Omega(\varsigma, v(\varsigma))\, d\varsigma \right\|_1$

Using (46) and the norm properties, it follows that

$$\|z(t) - v(t)\|_1 \leq a_1 + \frac{1}{\Gamma(\alpha)} \int_0^t (t-\varsigma)^{\alpha-1} \left| \Omega(\varsigma, z(\varsigma)) - \Omega(\varsigma, v(\varsigma)) \right| d\varsigma \tag{50}$$

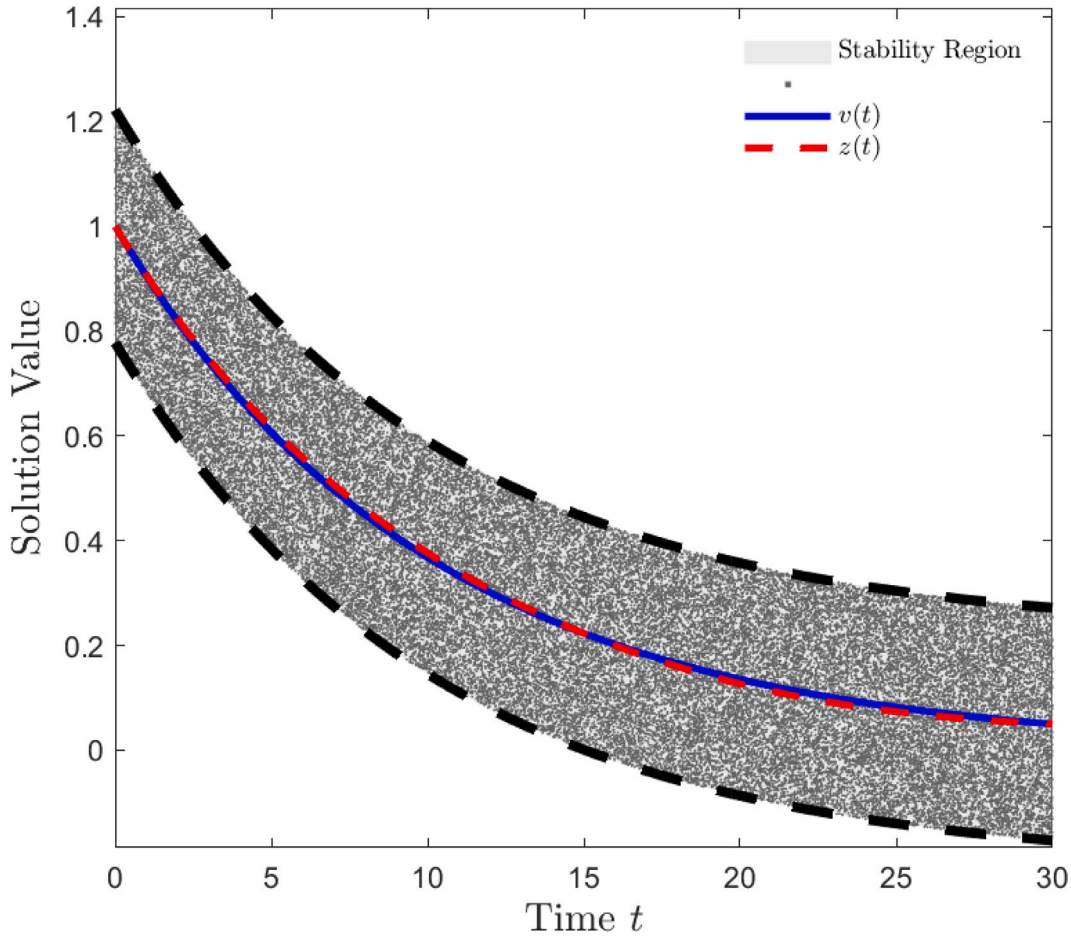


**Fig. 11.** Illustration of the exact solution $z(t)$, the perturbed solution $v(t)$, and the bounded stability region showing Hyers–Ulam tolerance under fractional perturbation.

Which is equivalent to

$$\|z(t) - v(t)\|_1 \leq \frac{\varrho T^\alpha}{\Gamma(\alpha+1)} + \frac{1}{\Gamma(\alpha)} \int_0^t (t-\varsigma)^{\alpha-1} \left|\Omega(\varsigma, z(\varsigma)) - \Omega(\varsigma, v(\varsigma))\right| \, d\varsigma \tag{51}$$

Applying the Contraction Mapping Principle as used in [11,61,62] yields

$$\|z(t) - v(t)\|_1 \leq \frac{\varrho T^\alpha}{\Gamma(\alpha+1)} + \frac{\eta T^\alpha}{\Gamma(\alpha+1)} \|z(t) - v(t)\|_1 \tag{52}$$

Through algebraic manipulation, we obtain the inequality $\chi\varrho \geq \|z(t) - v(t)\|_1$, where $\chi = \dfrac{T^\alpha}{\Gamma(\alpha+1) - \eta T^\alpha}$. Following Definition 10, let $\chi > 0$, under the condition that $\Gamma(\alpha+1) - \eta T^\alpha > 0$, which implies that $\Gamma(\alpha+1) > \eta T^\alpha$. Consequently, the fractional model (40) demonstrates Hyers–Ulam stability over the interval $[0, T]$, confirming its robustness in predicting epidemic dynamics over time. Small changes in control measures, such as modifications to vaccination or treatment rates, will not cause significant disruptions in the model's long-term behavior. This ensures the system remains stable and predictable, with minor adjustments in interventions not leading to unpredictable shifts in the epidemic. Therefore, the model provides reliable predictions for HPV transmission, maintaining stability at either PFE or endemic equilibrium, despite slight variations in control strategies as depicted in Fig. 11. □

### 2.8. Adam–Bashforth–Moulton (ABM) predictor–corrector scheme

The ABM method is widely used for solving fractional-order initial value problems (IVPs) due to its effectiveness. The Adams PECE method is particularly favored because it requires fewer function evaluations, making it more efficient and reliable compared to other techniques like extrapolation methods. By using the Predictor Corrector approach, the double-step method addresses the error estimation limitations typically found in one-step methods, such as Runge–Kutta [30,63]. As Adams–Bashforth method, the Adams–Moulton technique, allows for step size adjustments and method ordering to manage error control. This approach is more efficient than one-step methods, like the Milne method, by reducing unnecessary computations and time, leading to notable improvements in computational performance compared to multi-step methods [64,65].

Consider a fractional differential equation of the form:

$$^{C}_{t_0}D^\alpha_t v(t) = \Omega_i(t, v_i(t)), \quad t \geq 0, \quad \text{with} \quad v_i^n(0) = v_{i0} \in \mathbb{R}_+, \quad n = 0, 1, 2, \ldots, \quad i \in \mathbb{N}. \tag{53}$$

One can numerically solve for $v(t)$ at discrete time points using the PECE method.

$$v_i(t) = \alpha \sum_{n=0}^{\infty} \frac{v_{i0} t^n}{n!} + \frac{1}{\Gamma(\alpha)} \int_0^t (t-\xi)^{\alpha-1} \Omega_j(\xi, v_i(\xi))\, d\xi, \quad i \in \mathbb{N}. \tag{54}$$

### 2.8.1. Predictor step (Adams–Bashforth)

In the predictor step, we use an explicit Adam–Bashforth method, to predict the value of $v_i(t)$ based on the initial values, for a second-order Adams–Bashforth method (AB2), the predictor is:

$$\begin{cases}
S_f^{(c)}{}_{n+1}(t) = & S_f(0) + \frac{1}{\Gamma(\alpha)} \sum_{j=0}^{n} \beta_{j,n+1} \left( (1-\phi)\pi_f^\alpha - (\mu^\alpha + \lambda_m^\alpha) S_{fj}(t) \right), \\
V_{n+1}^{(c)}(t) = & V(0) + \frac{1}{\Gamma(\alpha)} \sum_{j=0}^{n} \beta_{j,n+1} \left( \phi\pi_f^\alpha - \mu^\alpha V_j(t) - (1-\delta)\lambda_m^\alpha V_j(t) \right), \\
E_f^{(c)}{}_{n+1}(t) = & E_f(0) + \frac{1}{\Gamma(\alpha)} \sum_{j=0}^{n} \beta_{j,n+1} \left( \lambda_m^\alpha S_{fj}(t) + (1-\delta)\lambda_m^\alpha V_j(t) - (\mu^\alpha + \gamma_f^\alpha) E_{fj}(t) \right) \\
I_f^{(c)}{}_{n+1}(t) = & I_f(0) + \frac{1}{\Gamma(\alpha)} \sum_{j=0}^{n} \beta_{j,n+1} \left( \gamma_f^\alpha E_{fj}(t) - (\mu^\alpha + \xi_f^\alpha) I_{fj}(t) \right), \\
R_f^{(c)}{}_{n+1}(t) = & R_f(0) + \frac{1}{\Gamma(\alpha)} \sum_{j=0}^{n} \beta_{j,n+1} \left( \eta\xi_f^\alpha I_{fj}(t) + \tau^\alpha C_j(t) - \mu^\alpha R_{fj}(t) \right), \\
C_{n+1}^{(c)}(t) = & C(0) + \frac{1}{\Gamma(\alpha)} \sum_{j=0}^{n} \beta_{j,n+1} \left( (1-\eta)\xi_f^\alpha I_{fj}(t) - (\mu^\alpha + d^\alpha + \tau^\alpha) C_j(t) \right), \\
S_m^{(c)}{}_{n+1}(t) = & S_m(0) + \frac{1}{\Gamma(\alpha)} \sum_{j=0}^{n} \beta_{j,n+1} \left( \pi_m^\alpha - (\mu^\alpha + \lambda_f^\alpha) S_{mj}(t) \right), \\
E_m^{(c)}{}_{n+1}(t) = & E_m(0) + \frac{1}{\Gamma(\alpha)} \sum_{j=0}^{n} \beta_{j,n+1} \left( \lambda_f^\alpha S_{mj}(t) - (\mu^\alpha + \gamma_m^\alpha) E_{mj}(t) \right), \\
I_m^{(c)}{}_{n+1}(t) = & I_m(0) + \frac{1}{\Gamma(\alpha)} \sum_{j=0}^{n} \beta_{j,n+1} \left( \gamma_m^\alpha E_{mj}(t) - (\mu^\alpha + \xi_m^\alpha) I_{mj}(t) \right), \\
R_m^{(c)}{}_{n+1}(t) = & R_m(0) + \frac{1}{\Gamma(\alpha)} \sum_{j=0}^{n} \beta_{j,n+1} \left( \xi_m^\alpha I_{mj}(t) - \mu^\alpha R_{mj}(t) \right).
\end{cases} \tag{55}$$

Whereby, $\beta_{j,n+1} = \frac{h^\alpha}{\alpha} \{(n+1-j)\alpha - (n-j)\alpha\}, \quad 0 \le j \le n.$

### 2.8.2. Corrector step in the PECE method

The corrector step refines the initial prediction (55) by using the Adam–Bashforth–Moulton (ABM) to adjust the solution. It iteratively improves the predicted value, reducing errors and enhancing accuracy.

$$\begin{cases}
S_{fn+1}(t) = & S_f(0) + \frac{h^\alpha}{\Gamma(\alpha+2)} \left( (1-\phi)\pi_f^\alpha - (\mu^\alpha + \lambda_m^\alpha) S_f^{(c)}{}_{n+1}(t) \right) \\
& + \frac{h^\alpha}{\Gamma(\alpha+2)} \sum_{j=0}^{n} \alpha_{j,n+1} \left( (1-\phi)\pi_f^\alpha - (\mu^\alpha + \lambda_m^\alpha) S_{fj}(t) \right), \\
V_{n+1}(t) = & V(0) + \frac{h^\alpha}{\Gamma(\alpha+2)} \left( \phi\pi_f^\alpha - \mu^\alpha V_{n+1}^{(c)}(t) - (1-\delta)\lambda_m^\alpha V_{n+1}^{(c)}(t) \right) \\
& + \frac{h^\alpha}{\Gamma(\alpha+2)} \sum_{j=0}^{n} \alpha_{j,n+1} \left( \phi\pi_f^\alpha - \mu^\alpha V_j(t) - (1-\delta)\lambda_m^\alpha V_j(t) \right), \\
E_{fn+1}(t) = & E_f(0) + \frac{h^\alpha}{\Gamma(\alpha+2)} \left( \lambda_m^\alpha S_f^{(c)}{}_{n+1}(t) + (1-\delta)\lambda_m^\alpha V_{n+1}^{(c)}(t) - (\mu^\alpha + \gamma_f^\alpha) E_f^{(c)}{}_{n+1}(t) \right) \\
& + \frac{h^\alpha}{\Gamma(\alpha+2)} \sum_{j=0}^{n} \alpha_{j,n+1} \left( \lambda_m^\alpha S_{fj}(t) + (1-\delta)\lambda_m^\alpha V_j(t) - (\mu^\alpha + \gamma_f^\alpha) E_{fj}(t) \right) \\
I_{fn+1}(t) = & I_f(0) + \frac{h^\alpha}{\Gamma(\alpha+2)} \left( \gamma_f^\alpha E_f^{(c)}{}_{n+1}(t) - (\mu^\alpha + \xi_f^\alpha) I_f^{(c)}{}_{n+1}(t) \right) \\
& + \frac{h^\alpha}{\Gamma(\alpha+2)} \sum_{j=0}^{n} \alpha_{j,n+1} \left( \gamma_f^\alpha E_{fj}(t) - (\mu^\alpha + \xi_f^\alpha) I_{fj}(t) \right), \\
R_{fn+1}(t) = & R_f(0) + \frac{h^\alpha}{\Gamma(\alpha+2)} \left( \eta I_f^{(c)}{}_{n+1}(t) + \tau^\alpha C_{n+1}^{(c)}(t) - \mu^\alpha R_f^{(c)}{}_{n+1}(t) \right) \\
& + \frac{h^\alpha}{\Gamma(\alpha+2)} \sum_{j=0}^{n} \alpha_{j,n+1} \left( \eta\xi_f^\alpha I_{fj}(t) + \tau^\alpha C_j(t) - \mu^\alpha R_{fj}(t) \right), \\
C_{n+1}(t) = & C(0) + \frac{h^\alpha}{\Gamma(\alpha+2)} \left( (1-\eta)\xi_f^\alpha I_f^{(c)}{}_{n+1}(t) - (\mu^\alpha + d^\alpha + \tau^\alpha) C_{n+1}^{(c)}(t) \right) \\
& + \frac{h^\alpha}{\Gamma(\alpha+2)} \sum_{j=0}^{n} \alpha_{j,n+1} \left( (1-\eta)\xi_f^\alpha I_{fj}(t) - (\mu^\alpha + d^\alpha + \tau^\alpha) C_j(t) \right), \\
S_{mn+1}(t) = & S_m(0) + \frac{h^\alpha}{\Gamma(\alpha+2)} \left( \pi_m^\alpha - (\mu^\alpha + \lambda_f^\alpha) S_m^{(c)}{}_{n+1}(t) \right) \\
& + \frac{h^\alpha}{\Gamma(\alpha+2)} \sum_{j=0}^{n} \alpha_{j,n+1} \left( \pi_m^\alpha - (\mu^\alpha + \lambda_f^\alpha) S_{mj}(t) \right), \\
E_{mn+1}(t) = & E_m(0) + \frac{h^\alpha}{\Gamma(\alpha+2)} \left( \lambda_f^\alpha S_m^{(c)}{}_{n+1}(t) - (\mu^\alpha + \gamma_m^\alpha) E_m^{(c)}{}_{n+1}(t) \right) \\
& + \frac{h^\alpha}{\Gamma(\alpha+2)} \sum_{j=0}^{n} \alpha_{j,n+1} \left( \lambda_f^\alpha S_{mj}(t) - (\mu^\alpha + \gamma_m^\alpha) E_{mj}(t) \right), \\
I_{mn+1}(t) = & I_m(0) + \frac{h^\alpha}{\Gamma(\alpha+2)} \left( \gamma_m^\alpha E_m^{(c)}{}_{n+1}(t) - (\mu^\alpha + \xi_m^\alpha) I_m^{(c)}{}_{n+1}(t) \right) \\
& + \frac{h^\alpha}{\Gamma(\alpha+2)} \sum_{j=0}^{n} \alpha_{j,n+1} \left( \gamma_m^\alpha E_{mj}(t) - (\mu^\alpha + \xi_m^\alpha) I_{mj}(t) \right), \\
R_{mn+1}(t) = & R_m(0) + \frac{h^\alpha}{\Gamma(\alpha+2)} \left( \xi_m^\alpha I_m^{(c)}{}_{n+1}(t) - \mu^\alpha R_m^{(c)}{}_{n+1}(t) \right) \\
& + \frac{h^\alpha}{\Gamma(\alpha+2)} \sum_{j=0}^{n} \alpha_{j,n+1} \left( \xi_m^\alpha I_{mj}(t) - \mu^\alpha R_{mj}(t) \right).
\end{cases} \tag{56}$$

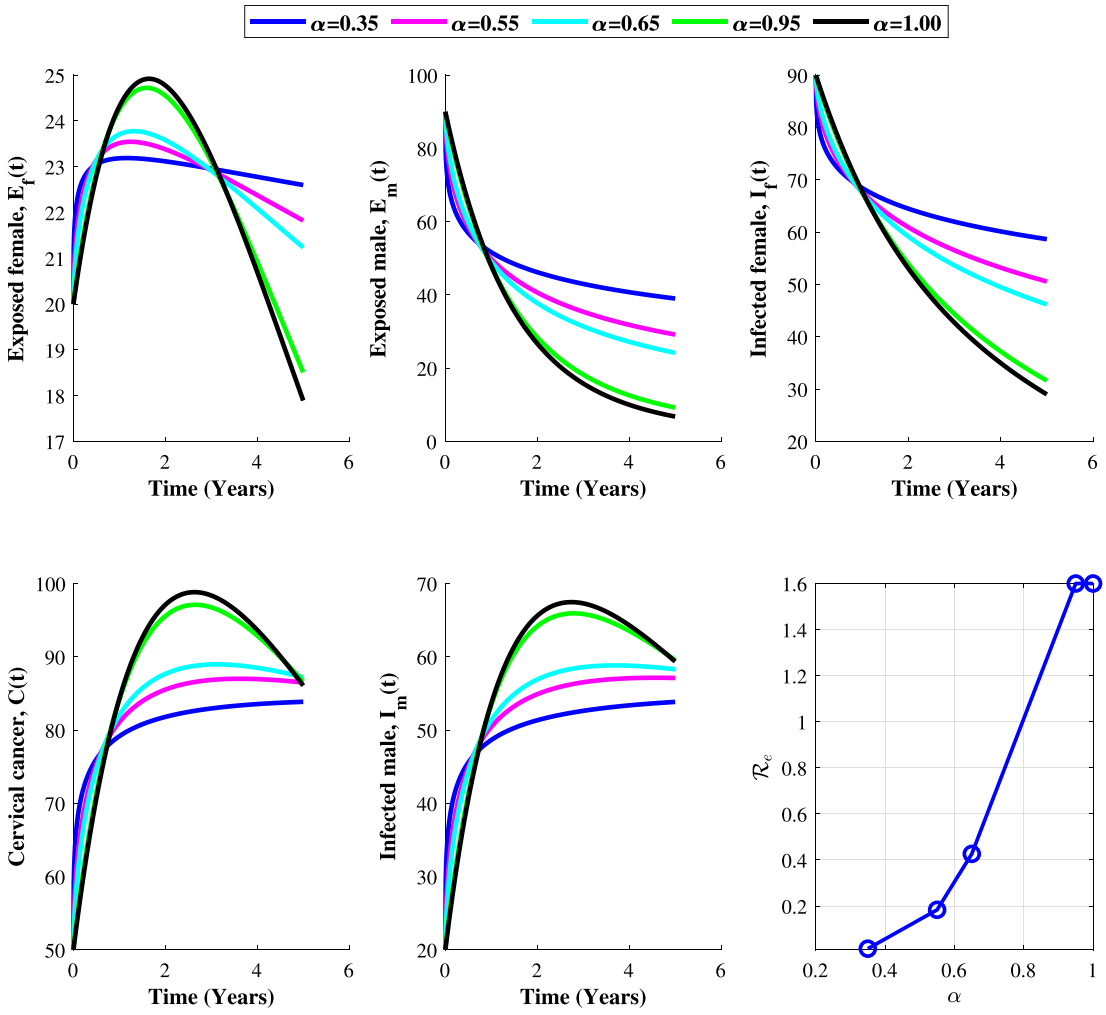


**Fig. 12.** Selection of $\alpha$ based on its ability to reduce the $\mathcal{R}_e$ below unity, reflecting real-world HPV dynamics.

$$\text{Whereby, } \alpha_{j,n+1} = \begin{cases} n^{\alpha+1} - (n-\alpha)(n+1)^{\alpha}, & \text{if} \quad j = 0, \\ (n-j+2)^{\alpha+1} + (n-j)^{\alpha+1} - 2(n-j+1)^{\alpha+1}, & \text{if} \quad 0 \le j \le n, \\ 1, & \text{if} \quad j = 1. \end{cases}$$

### *2.9. Numerical results and discussions*

In this section, we conduct numerical experiments of the FSM model (13) using MATLAB R2024a software to validate the earlier analytical results. For numerical approximation of fractional derivatives, we employ the Adam–Bashforth–Moulton (ABM) scheme, implemented in the MATLAB code `fde12`. This code uses a predictor–corrector PECE method based on the ABM scheme, as described in [30,63,66]. For further discussion on the convergence and accuracy of the numerical method, readers are referred to [27,30,67], while additional details on the stability of predictor–corrector algorithms for fractional differential equations can be found in [11,30,59].

The baseline parameter values from Table 2 and [1,9,56] are used to facilitate the simulations. The initial values for the sub-populations are set as $S_f(0) = 5365499$, $V(0) = 600000$, $E_f(0) = 100000$, $I_f(0) = 60000$, $R_f(0) = 20$, $C(0) = 10868$, $S_m(0) = 5365499$, $E_m(0) = 1000$, $I_m(0) = 60$, $R_m(0) = 0$. The selection of the fractional order, $\alpha$, is based on its ability to reduce the effective reproduction number ($\mathcal{R}_e$) to below one, which is a critical threshold for disease control. To ensure an accurate reflection of the real-world scenario, we use the same variables that were used to calculate Re. As we transition from integer-order to fractional-order models, incorporating the Caputo derivative, we observe a decrease in $\mathcal{R}_e$. When $\alpha$ reaches 0.35, $\mathcal{R}_e$ drops to 0.015, which is considered the measure of Papillomavirus-Free Equilibrium (PFE). At this stage, we can confidently conclude that the memory effect, integrated through the fractional-order approach, has been effectively captured, providing a more realistic and accurate representation of HPV dynamics. The memory effect is crucial for understanding how past events, such as previous infections or vaccination campaigns, impact current and future HPV transmission, as illustrated in Fig. 12 for further details.

#### *2.9.1. The role of memory effects on HPV dynamics*

To better understand the concept of the memory effect, it is helpful to describe it in terms of the derivative order $\alpha$ within the range $0 < \alpha \le 1$. When $\alpha = 1$, the system is memoryless, which corresponds to the classical (integer-order) calculus. As $\alpha$ decreases from 1 towards 0, the memory effect intensifies. The memory effect becomes less significant as $\alpha$ approaches 1, but it grows stronger as $\alpha$ moves further from 1.

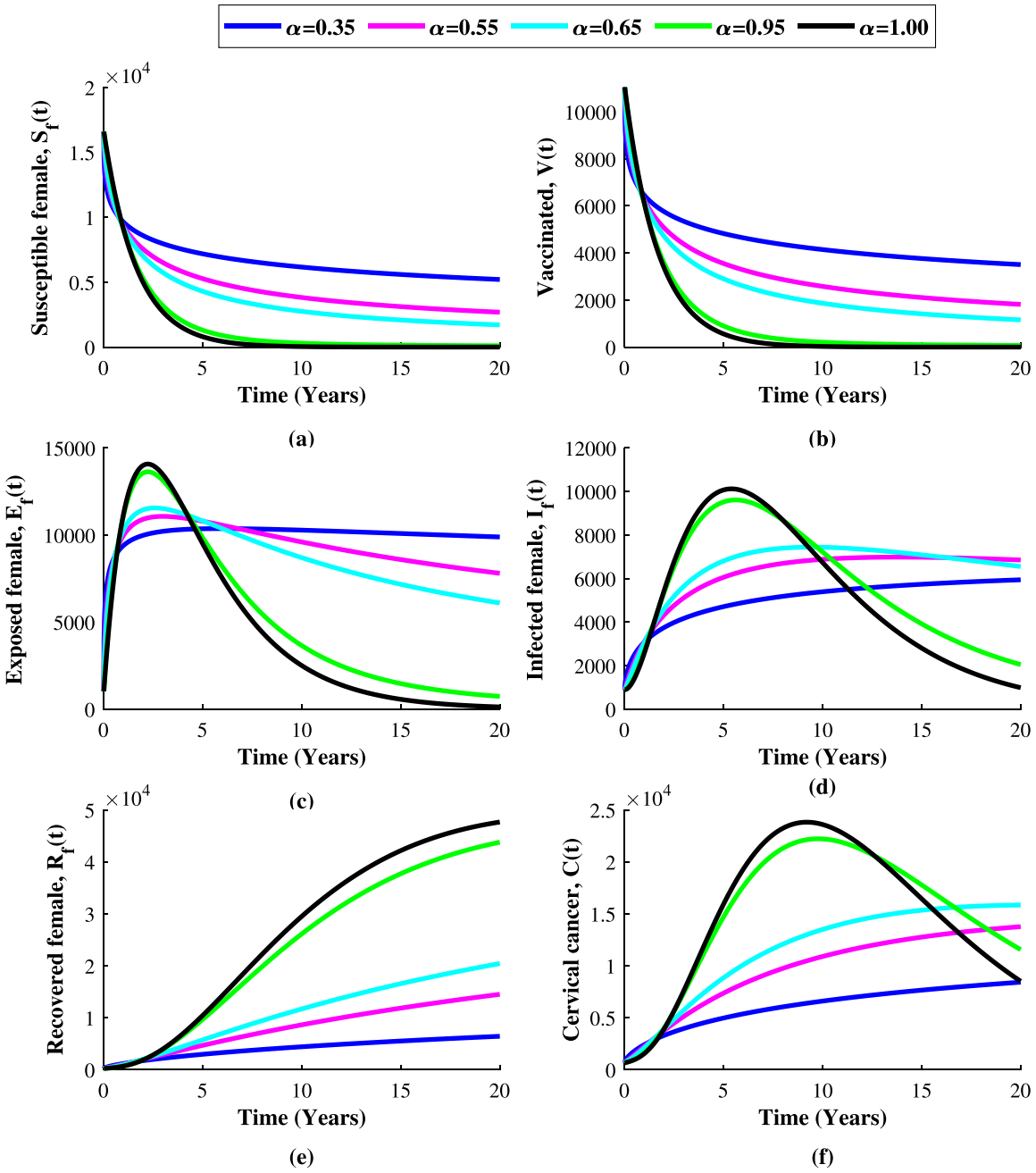


**Fig. 13.** Impact of varying memory parameter on female HPV transmission dynamics.

Figs. 13(a)–(f) and 14(a)–(d) illustrate how the system dynamics change as the fractional order $\alpha$ decreases from 1 to 0.35, reflecting the impact of the Caputo derivative and memory effects on disease transmission. Specifically, Figs. 13(a) and (b) show an increase in the susceptible and vaccinated female populations as the memory effect increases from 1 to 0.35. Figs. 13(d) and (f) demonstrate that as memory increases, the HPV-infected female population and the number of females suffering from cervical cancer decrease. Similarly, Figs. 14(c) and (d) reveal a decline in both the HPV-infected male population and the number of males who have recovered from HPV infections with higher memory.

These findings emphasize that incorporating the memory effect ($\alpha$) through the Caputo derivative significantly reduces HPV cases across various compartments, as shown in Figs. 13 and 14. In contrast, when there is no memory ($\alpha = 1$), more cases are observed, suggesting that individuals are not influenced by past infection dynamics or control strategies. These results align with other studies, reinforcing the importance of memory effects in accurately modeling and managing epidemic spread [9,11,68,69].

*2.9.2. Parameter variation of FSM (13) and $\mathcal{R}_e$, highlighting key drivers of $\mathcal{R}_e$ reduction*

Figs. 15–19 illustrate the impact of various intervention strategies on HPV infection dynamics and cervical cancer progression under a fractional-order framework.

Fig. 15 examines the role of vaccine efficacy at a fixed fractional order ($\alpha = 0.35$), highlighting its impact across key variables. Infected females ($I_f(t)$) show a substantial decline in HPV infections as vaccine efficacy increases, underscoring the role of vaccination in reducing HPV prevalence.

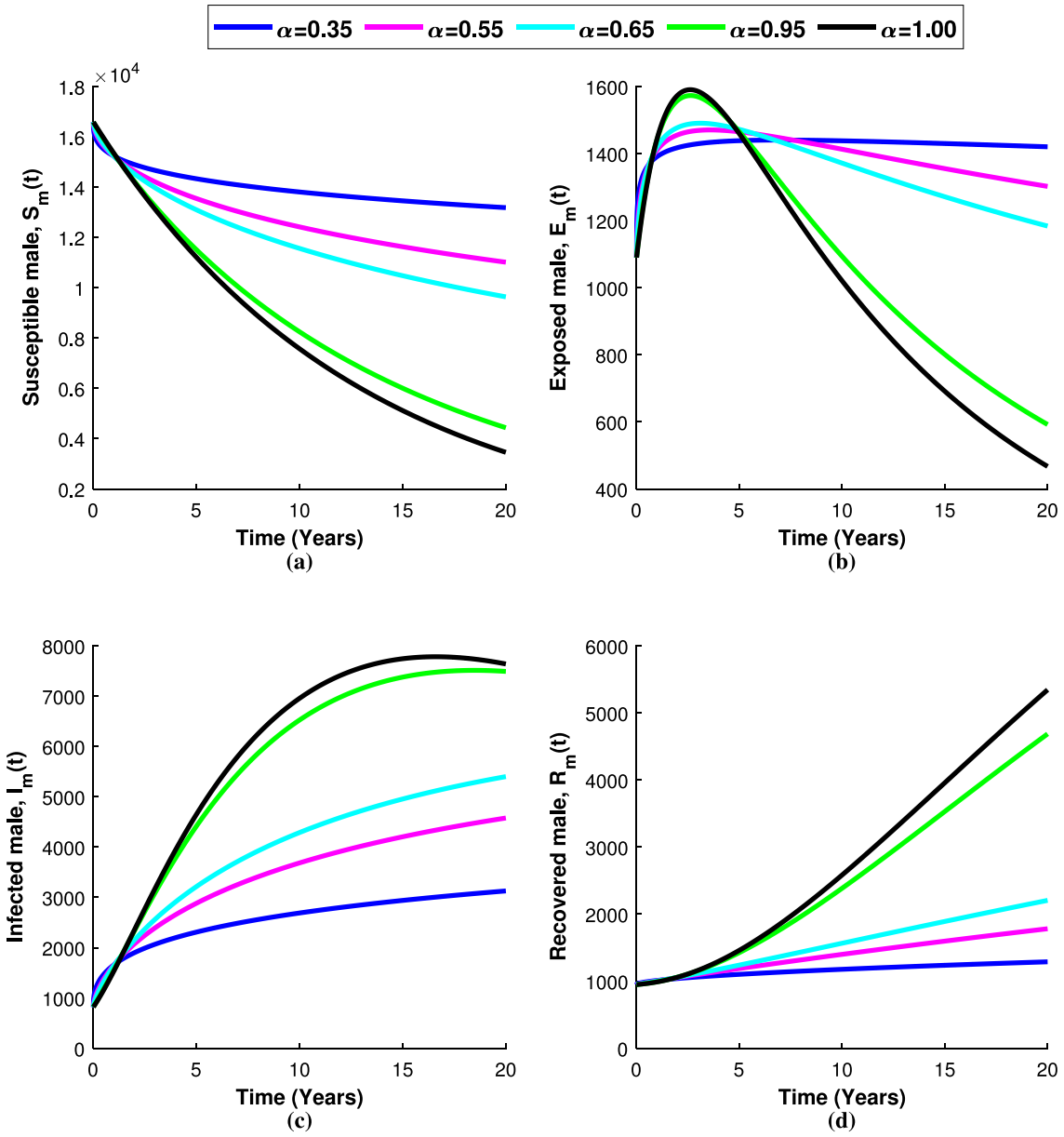


**Fig. 14.** Impact of varying memory parameter on male HPV transmission dynamics.

Similarly, cervical cancer cases ($C(t)$) decrease significantly, emphasizing that higher vaccine efficacy directly correlates with a lower incidence of cervical cancer. Additionally, the number of vaccinated individuals ($V(t)$) steadily rises, reinforcing the idea that effective vaccines contribute to greater population immunity. These findings collectively highlight the importance of increasing vaccine effectiveness in disease control, as higher efficacy not only prevents infections but also reduces the overall burden of cervical cancer.

Fig. 16 highlights the impact of treatment rates on key epidemiological variables. The representation of recovered individuals ($R_f(t)$) illustrates that an increase in treatment rates results in a substantial rise in recovery cases. Simultaneously, the depiction of cervical cancer cases ($C(t)$) reveals that higher treatment rates lead to a noticeable reduction in cervical cancer prevalence. These findings underscore the pivotal role of effective and timely treatment in mitigating HPV progression and improving health outcomes.

Fig. 17 specifically analyzes how varying natural recovery rates affect HPV infection dynamics, revealing that higher natural recovery rates contribute to a decline in the number of infected individuals while increasing recovery cases. This underscores the significance of natural immunity in disease management.

Fig. 18 evaluates the combined effects of vaccine efficacy and treatment rates, showing that a dual strategy enhancing vaccine effectiveness while increasing treatment coverage yields the most substantial reductions in HPV infections and cervical cancer cases.

Fig. 19 highlights the influence of natural recovery, vaccine efficacy, vaccination rate, and treatment on the basic reproduction number ($\mathcal{R}_e$). Infected females ($I_f(t)$) show that an increase in these intervention measures leads to a steady decline in infections, demonstrating their collective role in reducing HPV transmission. Another key aspect focuses on recovered females ($R_f(t)$), indicating that higher vaccination rates and improved natural recovery contribute to an increase in recovered individuals over time, with past treatment effects also playing a role in shaping recovery outcomes. Additionally, the analysis of cervical cancer cases ($C(t)$) confirms that a well-integrated strategy combining vaccination, treatment,

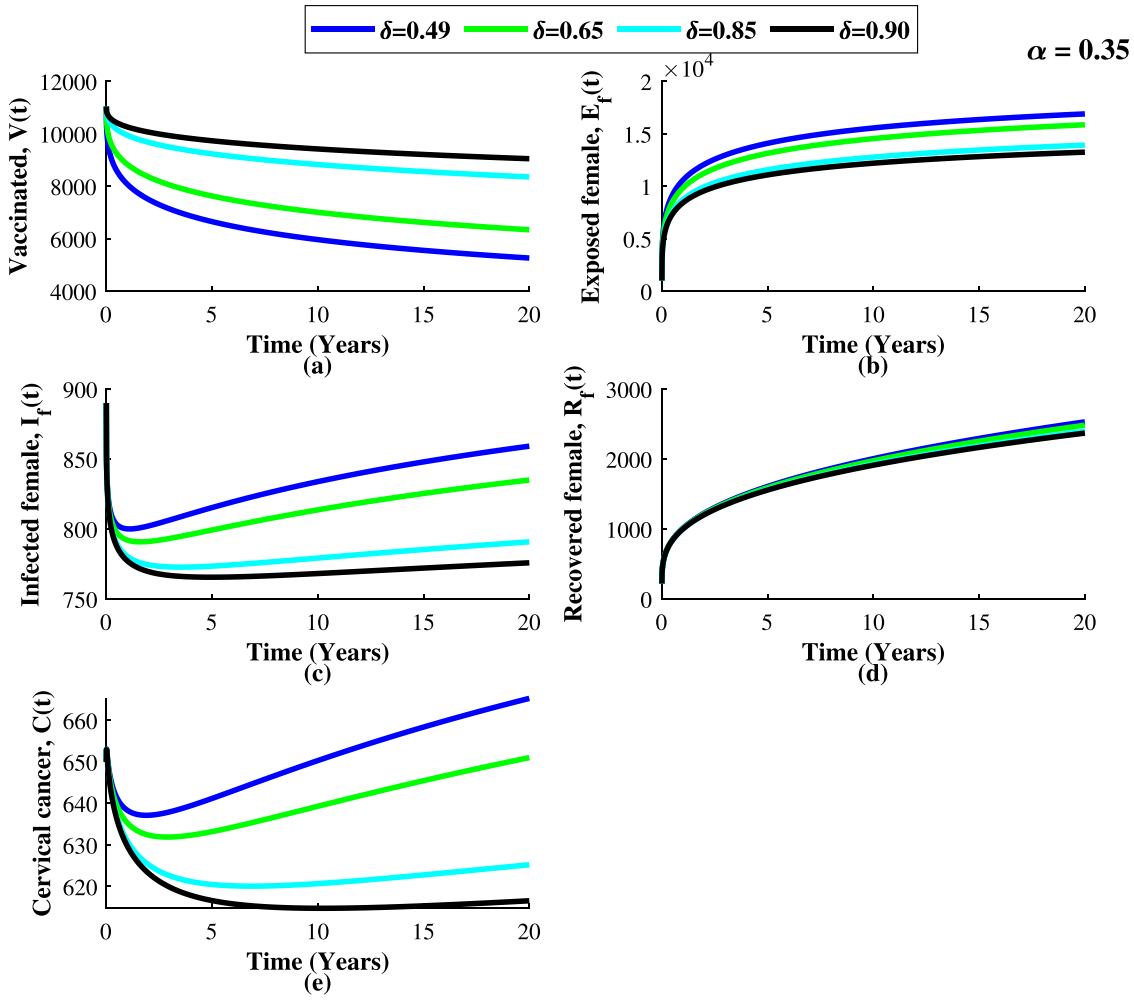


**Fig. 15.** Impact of varying vaccine efficacy at a fixed fractional order $\alpha = 0.35$.

and past recovery significantly lowers the number of individuals progressing to cervical cancer. These findings emphasize the necessity of a comprehensive public health approach that incorporates vaccination, treatment, and natural recovery, while considering the long-term effects of past interventions, to effectively curb HPV transmission and its associated health impacts.

The analysis highlights the combined effectiveness of vaccination, treatment, and natural recovery in controlling HPV transmission and reducing cervical cancer incidence. Figs. 15 to 19 illustrate key findings: Fig. 15 shows how increased vaccine efficacy significantly lowers HPV infections, while Fig. 16 demonstrates that higher treatment rates lead to more recoveries and reduced cervical cancer prevalence. Figs. 18 and 19 emphasize the synergistic impact of vaccination, treatment, and memory effects, with the latter enhancing disease control by incorporating past events. Finally, Fig. 17 reinforces the importance of integrating vaccination, treatment, and natural recovery for optimal disease control. These results underscore the need for a comprehensive, multi-faceted approach to HPV management.

Fig. 20 demonstrates that both vaccination coverage ($\phi$) and vaccine efficacy ($\delta$) are critical determinants in reducing the overall burden of cervical cancer within the population. A higher coverage rate ($\phi$) indicates that a greater proportion of the eligible population receives the vaccine, thereby decreasing $R_e$ and limiting the transmission dynamics of HPV. Similarly, a higher vaccine efficacy ($\delta = 0.455556$), as reported in Table 2, reflects improved immunogenicity, which substantially lowers the probability of progression from HPV infection to cervical cancer. The synergistic impact of high coverage and high efficacy yields the most significant reduction in disease incidence. The optimal strategy, as illustrated in Fig. 20, suggests that targeting a vaccination coverage of $\phi = 0.56667$ among eligible individuals maximally reduces HPV infections. This highlights the epidemiological importance of implementing comprehensive immunization programs that ensure both widespread vaccine uptake and high vaccine performance to effectively control cervical cancer and minimize the associated public health burden.

Fig. 21 demonstrates the synergistic effect of natural recovery ($\eta$) and treatment rate ($\tau$) on the increase in the number of recovered female individuals over time. As both parameters increase, there is a marked rise in the proportion of women recovering from HPV-related infections, suggesting that more individuals are successfully clearing the virus before it advances to cervical cancer. Higher vaccine efficacy strengthens immune protection, either preventing infection or mitigating its severity, while an elevated treatment rate ensures timely medical intervention, thereby accelerating recovery. This combined effect significantly enhances the recovered population, underscoring the epidemiological value of integrating effective vaccination with comprehensive treatment strategies to reduce disease progression and improve women's health outcomes.

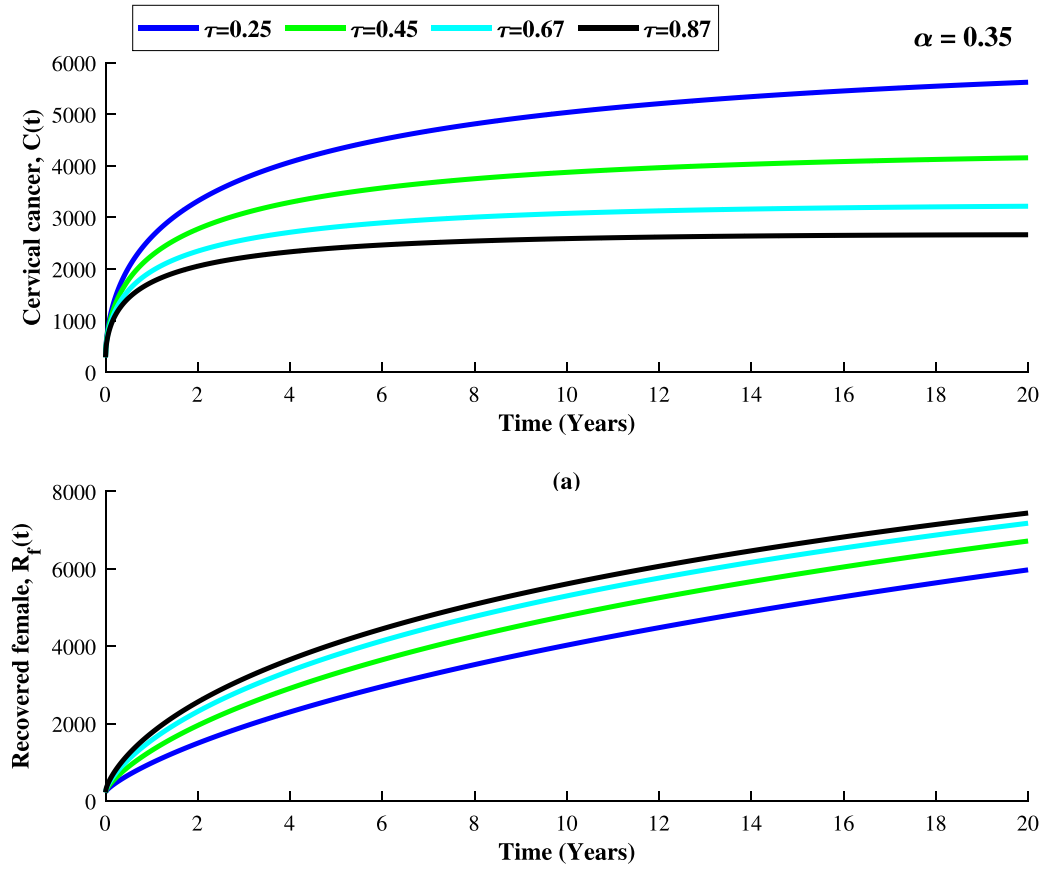


**Fig. 16.** Impact of varying treatment rate at a fixed fractional order $\alpha = 0.35$.

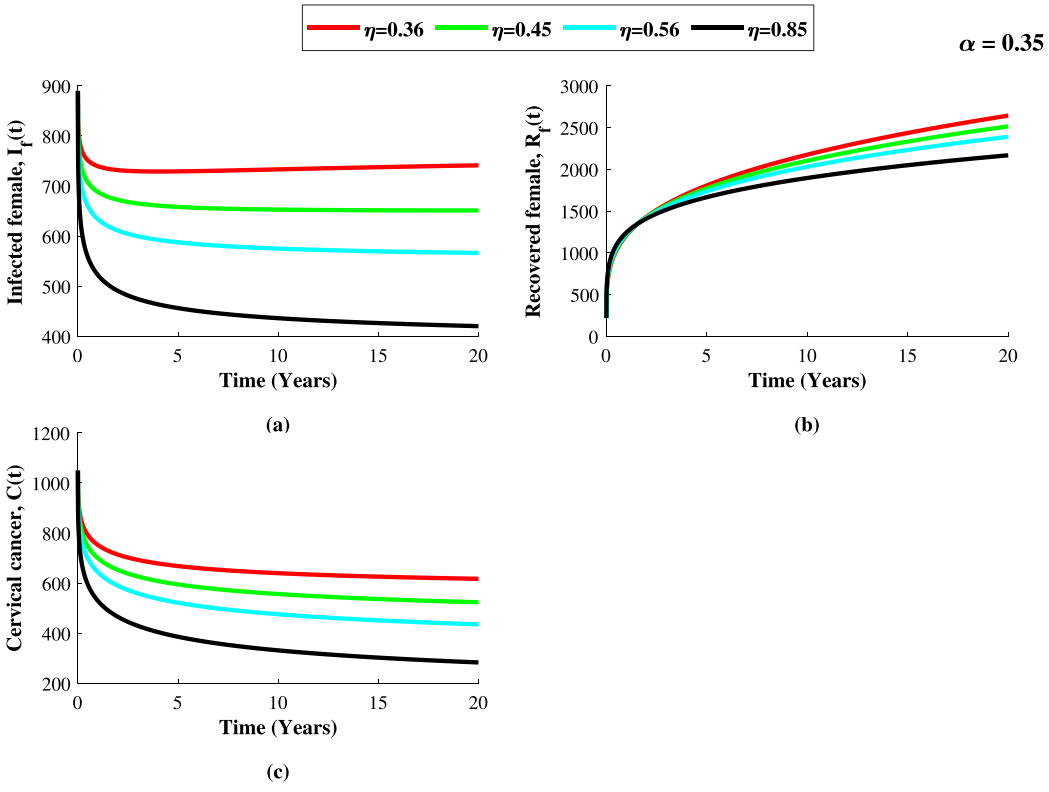


**Fig. 17.** Impact of varying natural recovery on Female HPV Infection Dynamics at a fixed fractional order $\alpha = 0.35$.

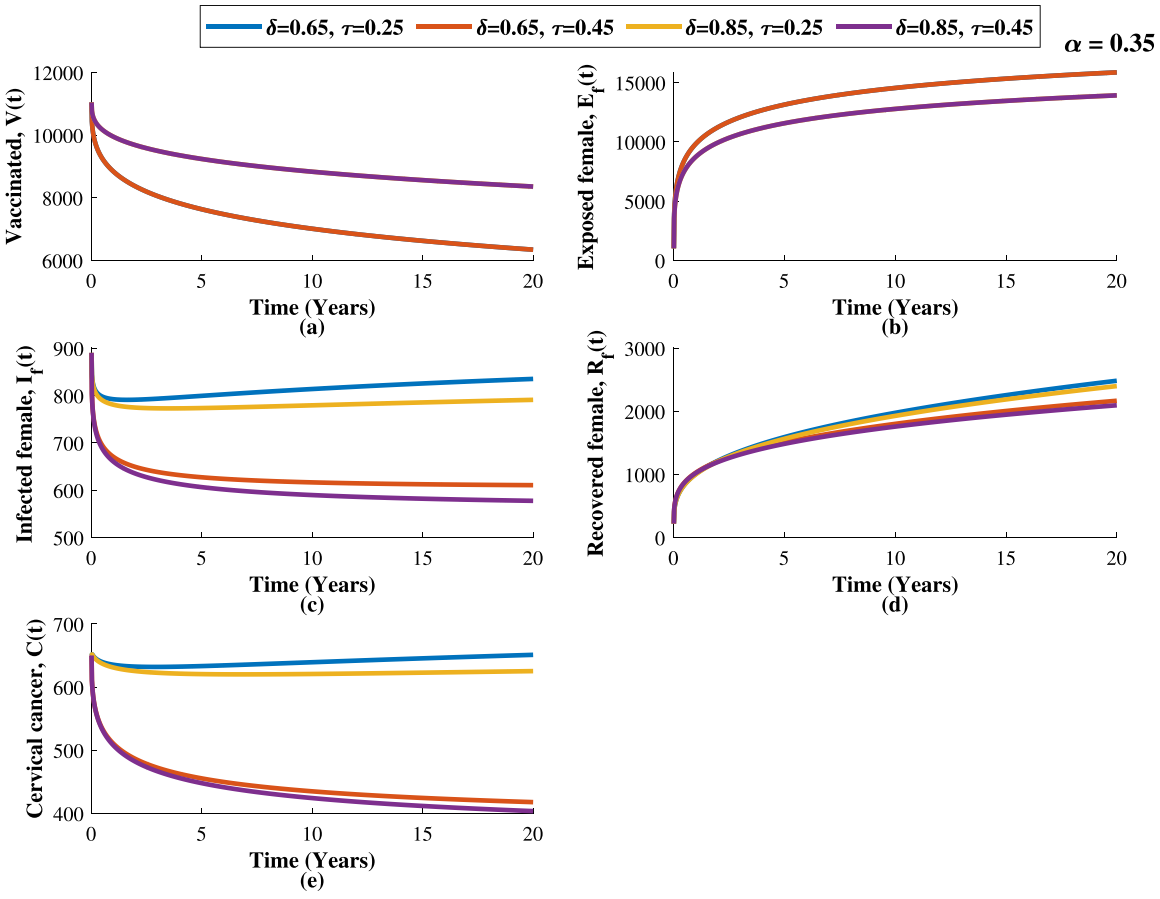


**Fig. 18.** Impact of varying vaccine efficacy and treatment rate on female HPV infection dynamics at a fixed fractional order of $\alpha = 0.35$.

## 3. Conclusion

This study introduces a novel fractional-order model for investigating the transmission dynamics of Human Papillomavirus (HPV) and its progression to cervical cancer. By employing the Caputo fractional derivative, the model incorporates memory effects to more accurately reflect biological realities compared to classical integer-order models. These memory effects capture the cumulative influence of historical events such as prior infections, treatments, and vaccination campaigns on current disease transmission dynamics. The model structure includes key compartments for vaccinated individuals, treated patients, and natural recoveries, enabling a more comprehensive evaluation of HPV control strategies.

Theoretical analysis established the positivity and boundedness of solutions, and the effective reproduction number ($\mathcal{R}_e$) was derived using a Graph Theoretic approach. Global stability of both the Papillomavirus-Free Equilibrium (PFE) and endemic equilibrium was proven using Lyapunov functional techniques. These findings were further validated through numerical simulations conducted via the Adams–Bashforth–Moulton (ABM) predictor–corrector method. Parameters were estimated using the Markov Chain Monte Carlo (MCMC) technique, and Partial Rank Correlation Coefficients (PRCC) were used for global sensitivity analysis. Key parameters including vaccination coverage, vaccine efficacy, and treatment rate were shown to critically influence $R_e$. Notably, an optimal fractional order ($\alpha = 0.35$) led to a significant reduction in $\mathcal{R}_e$ to 0.015, supporting the attainment of a stable PFE and underscoring the lasting impact of past interventions.

The ABM scheme was chosen due to its proven convergence and stability when applied to fractional-order differential equations, particularly those involving Caputo derivatives. This method, as validated in studies such as Garrappa [30,63], offers a PECE (Predict-Evaluate-Correct-Evaluate) structure that enhances both computational efficiency and numerical accuracy. Its ability to support step-size adaptivity and handle historical memory makes it especially suitable for fractional epidemic models, including HPV, COVID-19 [11], and tuberculosis [62]. However, ABM requires smooth initial data and can be computationally intensive for long time horizons due to the non-local nature of fractional integrals. Despite these limitations, its strengths in modeling persistent infections justify its application here.

To enhance the applicability, realism, and robustness of the FSM model (13), future work could incorporate optimal control theory, behavioral dynamics, and population heterogeneity. Introducing time-dependent control variables for vaccination and treatment within an optimal control framework would allow for the identification of cost-effective strategies that minimize disease burden. These controls could reflect real-world intervention policies, including public health campaigns, and would help guide decision-makers in resource allocation. Additionally, integrating age structure, spatial heterogeneity, and media-induced behavioral change dynamics would provide a more detailed and accurate representation of the population's response to HPV interventions. Such improvements would support not only HPV modeling but also broader applications to other memory-influenced infections.

Recent advances, such as those proposed in [70,71], suggest that the integration of stochastic optimal control can significantly enhance model realism by accounting for uncertainties in intervention efficacy and population behavior. Applying similar strategies to the HPV model would allow for stochastic modeling of treatment rates, vaccine uptake, and education programs. Delay differential equations and stochastic perturbations, as

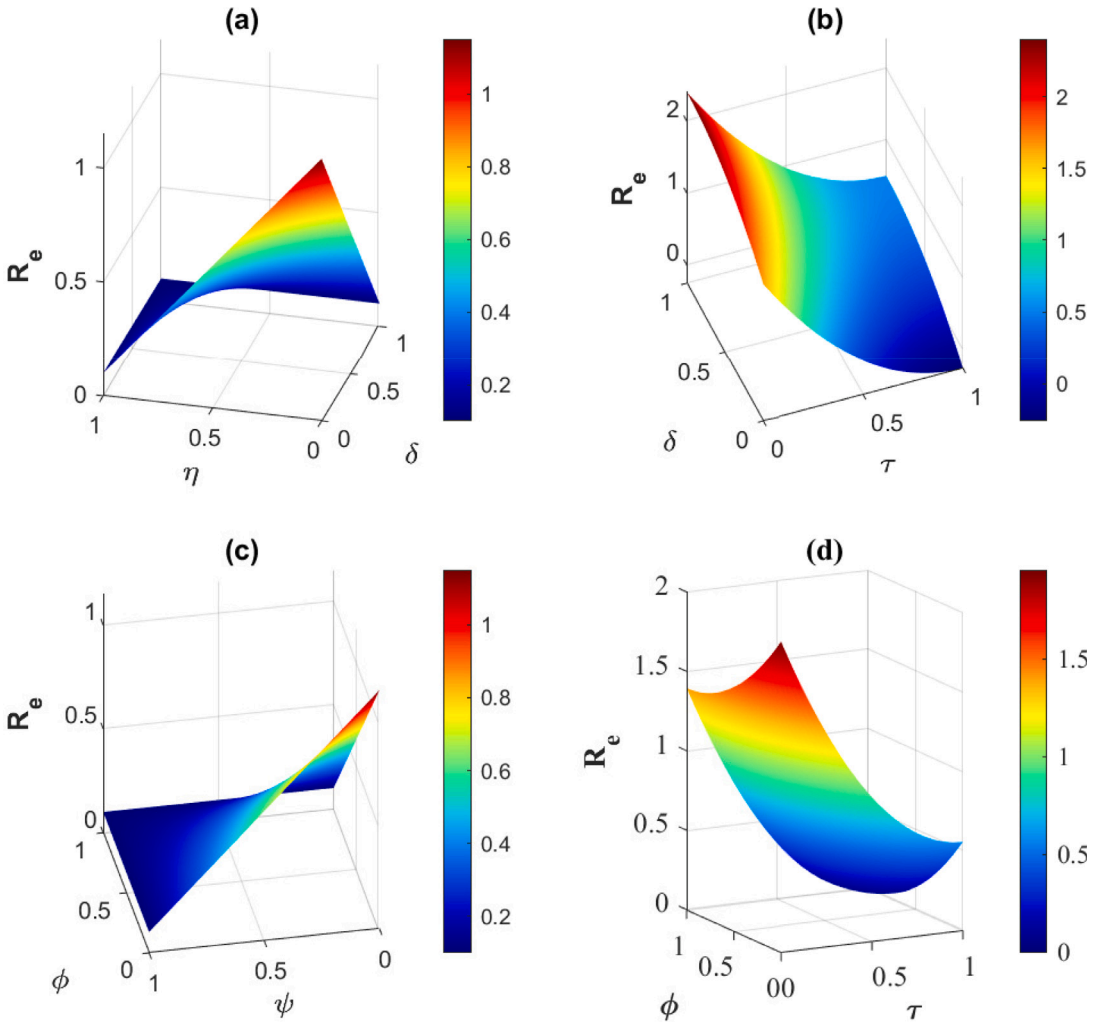


**Fig. 19.** Effect of varying natural recovery, vaccine efficacy, vaccination rate, and treatment on $\mathcal{R}_e$ at a fixed fractional order of $\alpha = 0.35$.

used in [72,73], can be incorporated to capture latency periods and random fluctuations in disease dynamics key features in real-world HPV transmission. Furthermore, inspired by [74], the use of Mittag-Leffler type fractional operators and coupled integral boundary conditions can generalize memory effects and improve the model's flexibility. These future extensions would contribute to better predictive performance and more resilient intervention strategies under uncertainty.

In our future work, we plan to extend the current fractional HPV vaccination and treatment model by incorporating stochastic optimal control strategies to evaluate the combined impact of education campaigns, vaccination timing, and treatment interventions under uncertainty. Drawing inspiration from the frameworks in [71,72], we aim also in another direction to introduce time delays to represent latency in vaccine response and treatment initiation, along with noise terms to simulate demographic or intervention-based variability. These modifications will allow us to develop a more flexible, data-driven model capable of informing robust and adaptive HPV control strategies tailored to real-world complexities.

## CRediT authorship contribution statement

**Sylas Oswald:** Writing – review & editing, Writing – original draft, Visualization, Validation, Software, Resources, Methodology, Investigation, Formal analysis, Data curation, Conceptualization. **Eunice Mureithi:** Writing – review & editing, Visualization, Validation, Supervision, Methodology, Funding acquisition, Formal analysis, Data curation. **Berge Tsanou:** Writing – review & editing, Visualization, Supervision, Software, Resources, Methodology, Funding acquisition, Formal analysis, Conceptualization. **Michael Chapwanya:** Writing – review & editing, Visualization, Validation, Supervision, Software, Resources, Methodology, Funding acquisition, Data curation, Conceptualization. **Crispin Kahesa:** Writing – review & editing, Visualization, Validation, Supervision, Methodology, Funding acquisition. **Kijakazi Mashoto:** Writing – review & editing, Validation, Supervision, Software, Resources, Methodology, Investigation, Funding acquisition, Formal analysis, Conceptualization.

## Ethics approval and consent participate

I would like to clarify that we did not use any data requiring approval or consent from individuals involved in data acquisition. The data utilized in our work were obtained from relevant articles and properly cited.

**Funding statement**

This study was fully funded by Bill & Melinda Gates Foundation.

**AI Acknowledgment**

We hereby confirm that no artificial intelligence (AI) tools or algorithms were used in the generation of this work, including data analysis, model formulation, model analysis, or numerical simulation. This is an original work of the authors, and all aspects of the study were conducted using traditional research methods and manual analysis.

**Declaration of competing interest**

The authors declare that they have no known competing financial interests or personal relationships that could have appeared to influence the work reported in this paper.

**Acknowledgments**

This research was conducted at the Department of Mathematics, University of Dar es Salaam, as part of the Central and Eastern Africa Female Health Oriented Modeling Epidemics Consortium (CAF-HOMEC) Project, with generous support from the Bill & Melinda Gates Foundation, United States (Grant No. INV-022584). The views, findings, conclusions, and recommendations expressed herein are solely those of the authors and do not necessarily reflect those of the funding organization. The authors also wish to sincerely thank the anonymous reviewers for their insightful comments and suggestions, which significantly improved the quality of this work.

**Data availability**

The findings of this study are based on synthetic data and published epidemiological studies, as outlined in Table 2. The parameters were estimated using these sources, and all data and model estimates are thoroughly documented in the manuscript to ensure transparency for replication and further analysis.

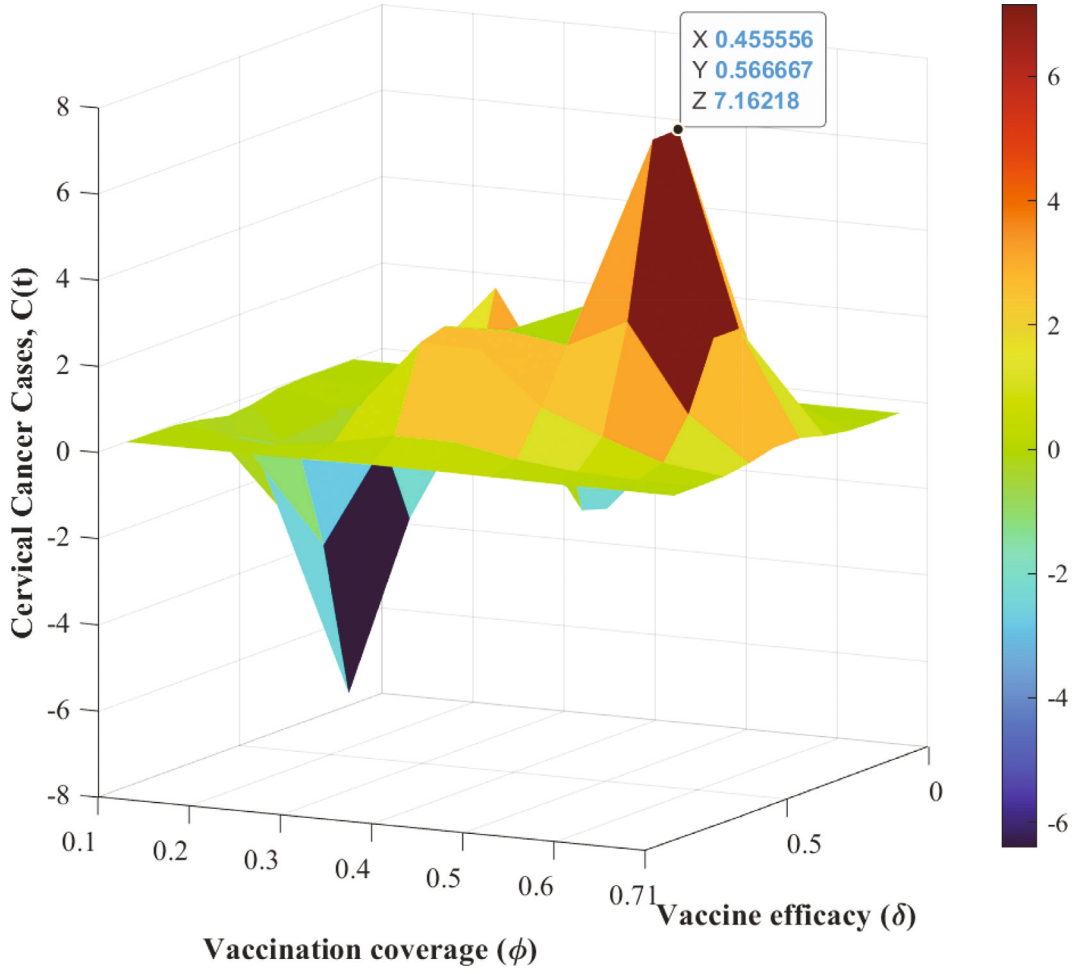


**Fig. 20.** Optimal combination of vaccine coverage ($\phi$) and vaccine efficacy ($\delta$).

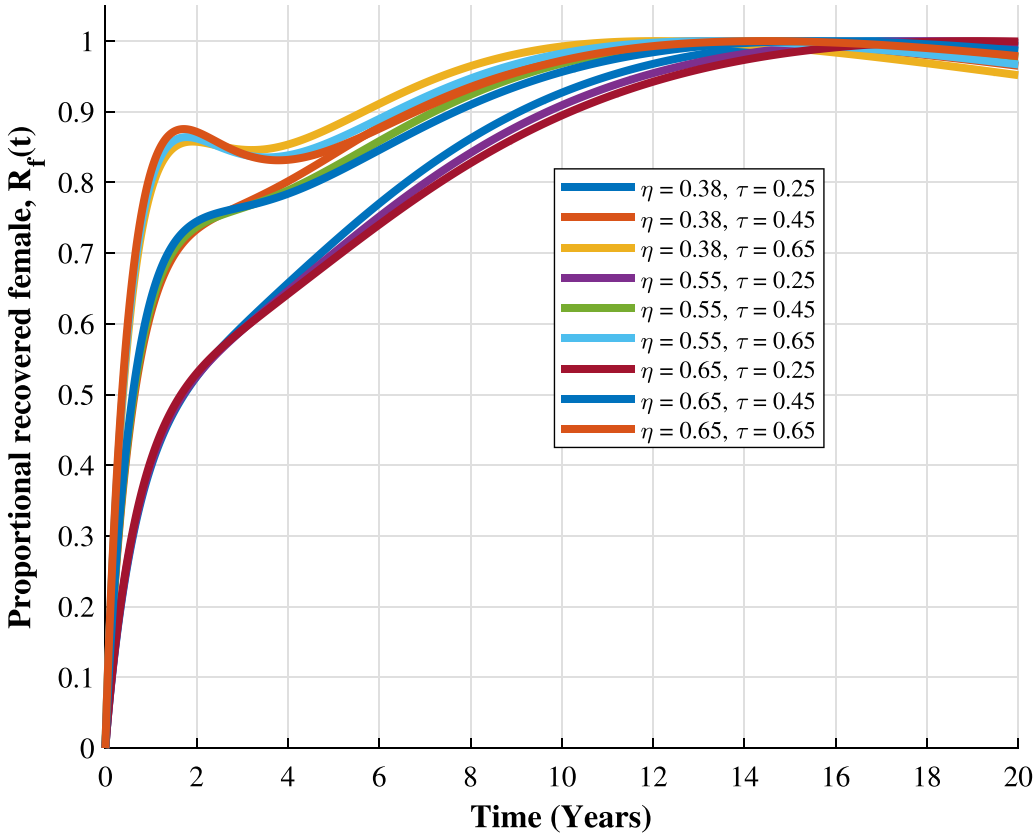


**Fig. 21.** Varying natural recovery and treatment on $\mathcal{R}_e$ at a fixed fractional order of $\alpha = 0.35$.

## References


[1] NCTG, National cancer treatment guidelines, 2020, https://www.orci.or.tz/oagrydee/2020/02/National-Cancer-Treatment-Guidelines.pdf. (Accessed 23 July 2024).

[2] D. Guillaume, J.G. Rosen, L.B. Mlunde, B.J. Njiro, C. Munishi, D. Mlay, A. Gerste, T.A. Holroyd, M.R. Giattas, C. Morgan, B.F. Sunguya, Acceptability of an integrated school-based HPV vaccination program within two districts of Tanzania: a qualitative descriptive study, PLOS Glob. Public Heal. 3 (1) (2023) e0001394.

[3] J. Ferlay, M. Ervik, F. Lam, M. Laversanne, M. Colombet, L. Mery, M. Piñeros, A. Znaor, I. Soerjomataram, F. Bray, Global cancer observatory: International agency for research on cancer, 2024, https://gco.iarc.who.int/media/globocan/factsheets/populations/834-tanzania-united-republic-of-fact-sheet.pdf. (Accessed 7 September 2024).

[4] K.J. Baisley, A. Andreasen, J. Irani, S. Nnko, J. Changalucha, T. Crucitti, S. Francis, C.H. Hansen, R.J. Hayes, A. Buvé, D. Watson-Jones, HPV prevalence around the time of sexual debut in adolescent girls in Tanzania, Sex. Transm. Infect. 96 (3) (2020) 211–219.

[5] K. Abbas, K.J. Yoo, K. Prem, M. Jit, Equity impact of HPV vaccination on lifetime projections of cervical cancer burden among cohorts in 84 countries by global, regional, and income levels, Eclinicalmedicine 70 (2024).

[6] L. Leandry, E.W. Mureithi, An investigation on the monkeypox virus dynamics in human and rodent populations for a deterministic mathematical model, Inform. Med. Unlocked 41 (2023) 101325.

[7] I. Sosoma, E. Mureithi, G. Alendal, Z. Makondo, N.S. Mbare, A data-driven dynamical system model for assessing targeted interventions against brucellosis in Tanzania, Comp. Immunol. Microbiol. Infect. Dis. (2025) 102324.

[8] Chunya Liu, Hua Liu, Xinjie Zhu, Xiaofen Lin, Qibin Zhang, Yumei Wei, Dynamic analysis of human papillomavirus transmission model under vaccine intervention: a case study of cervical cancer patients from Hungary, Adv. Contin. Discret. Model. 2024 (1) (2024) 36.

[9] Sylas Oswald, Eunice Mureithi, Berge Tsanou, Michael Chapwanya, Kijakazi Mashoto, Crispin Kahesa, MCMC-driven mathematical modeling of the impact of HPV vaccine uptake in reducing cervical cancer, Sci. Afr. (2025) e02633.

[10] Sung Eun Choi, Abhishek Choudhary, Jingyi Huang, Stephen Sonis, Anna R. Giuliano, Alessandro Villa, Increasing HPV vaccination coverage to prevent oropharyngeal cancer: a cost-effectiveness analysis, Tumour Virus Res. 13 (2022) 200234.

[11] Stephen Edward, A fractional order model for the transmission dynamics of shigellosis, Heliyon 10 (10) (2024).

[12] Samson Olaniyi, Sulaimon F. Abimbade, Furaha M. Chuma, Okunloye A. Adepoju, Olajumoke D. Falowo, A fractional-order tuberculosis model with efficient and cost-effective optimal control interventions, Decis. Anal. J. 8 (2023) 100324.

[13] Yustina Amon Liana, Jufren Zakayo Ndendya, Nyimvua Shaban, The nutritional nexus: Modeling the impact of malnutrition on TB transmission, Sci. Afr. e02516 (2025).

[14] Ivo Petráš, Fractional-Order Nonlinear Systems: Modeling, Analysis and Simulation, Springer Science & Business Media, 2011.

[15] A. El-Mesady, A.M.S. Mahdy, Fatma Özköse, A fractional-order model with prevention and isolation optimal control measures to reduce the transmission of tuberculosis, J. Taibah Univ. Sci. (2025).

[16] Hegagi Mohamed Ali, Amr M.S. Mahdy, A. El-Mesady, Investigation of stability criteria and optimal control measures for a fractional-order model of human papillomavirus infection and cervical cancer, Int. J. Biomath. (2025).

[17] Simphiwe M. Simelane, Justin B. Munyakazi, Phumlani G. Dlamini, Oluwaseun F. Egbelowo, Projections of human papillomavirus vaccination and its impact on cervical cancer using the Caputo fractional derivative, Math. Biosci. Eng. 20 (7) (2023) 11605–11626.

[18] Amr Elsonbaty, Tareq M. Al-Shami, A. El-Mesady, Unveiling the dynamics of meningitis infections: a comprehensive study of a novel fractional-order model with optimal control strategies, Bound. Value Probl. 2025 (48) (2025).

[19] A. El-Mesady, Abdulmuhsen Aldakhil, Amr Elsonbaty, On nonlinear dynamical analysis of a fractional-order two-strains Nipah virus model with optimal controls, Partial. Differ. Equ. Appl. Math. (2024).

[20] Ahmed El-Mesady, Hegagi Mohamed Ali, The influence of prevention and isolation measures to control the infections of the fractional Chickenpox disease model, Math. Comput. Simulation 226 (2024) 606–630.

[21] Waleed Adel, H. Günerhan, K.S. Nisar, P. Agarwal, A. El-Mesady, Designing a novel fractional order mathematical model for COVID-19 incorporating lockdown measures, Sci. Rep. 14 (2024) 2926.
[22] Jufren Zakayo Ndendya, Joshua A. Mwasunda, Stephen Edward, Nyimvua Shaban Mbare, A fractional-order model for rabies transmission dynamics using the Atangana–Baleanu–Caputo derivative and MCMC methods, Sci. Afr. 29 (2025) e02800.
[23] Jufren Zakayo Ndendya, Joshua A. Mwasunda, Stephen Edward, Nyimvua Shaban Mbare, A Caputo fractional-order model with MCMC for rabies transmission dynamics, Comput. Methods Programs Biomed.: Updat. 5 (2025) 100206.
[24] J.Z. Ndendya, E. Mureithi, J.A. Mwasunda, et al., Modelling the effects of quarantine and protective interventions on the transmission dynamics of Marburg virus disease, Model. Earth Syst. Env. 11 (2025) 81.
[25] Anatoli A. Kilbas, Hari M. Srivastava, Juan J. Trujillo, Theory and Applications of Fractional Differential Equations, vol. 204, Elsevier, 2006.
[26] Cruz Vargas-De-León, Volterra-type Lyapunov functions for fractional-order epidemic systems, Commun. Nonlinear Sci. Numer. Simul. 24 (1–3) (2015) 75–85.
[27] Kai Diethelm, Alan D. Freed, The FracPECE subroutine for the numerical solution of differential equations of fractional order, Forsch. Und Wiss. Rechn. 1999 (1998) 57–71.
[28] K. Diethelm, A.D. Freed, The frac PECE subroutine for the numerical solution of differential equations of fractional order, in: S. Heinzel, T. Plesser (Eds.), Forschung Und Wissenschaftliches Rechnen 1998, Gessellschaft fur Wissenschaftliche Datenverarbeitung, Gottingen, 1999, pp. 57–71.
[29] Sayed Murad Ali Shah, Hussan Tahir, Asaf Khan, Wajahat Ali Khan, Alishba Arshad, Stochastic model on the transmission of worms in wireless sensor network, J. Math. Tech. Model. 1 (1) (2024) 52–74.
[30] Roberto Garrappa, On linear stability of predictor–corrector algorithms for fractional differential equations, Int. J. Comput. Math. 87 (10) (2010) 2281–2290.
[31] Amr Elsonbaty, Waleed Adel, Yassine Sabbar, A. El-Mesady, Nonlinear dynamics and optimal control of a fractional order cotton leaf curl virus model incorporating climate change influences, Partial. Differ. Equ. Appl. Math. (2024).
[32] Zaid M. Odibat, Nabil T. Shawagfeh, Generalized Taylor's formula, Appl. Math. Comput. 186 (1) (2007) 286–293.
[33] Song Liang, Ranchao Wu, Liping Chen, Laplace transform of fractional order differential equations, Electron. J. Differential Equations 139 (2015) 2015.
[34] Li Kexue, Peng Jigen, Laplace transform and fractional differential equations, Appl. Math. Lett. 24 (12) (2011) 2019–2023.
[35] Wajahat Ali Khan, Rahat Zarin, Aurang Zeb, Yousaf Khan, Amir Khan, Navigating food allergy dynamics via a novel fractional mathematical model for antacid-induced allergies, J. Math. Tech. Model. 1 (1) (2024) 25–51.
[36] Abdelalim A. Elsadany, Yassine Sabbar, Waleed Adel, A. El-Mesady, Dynamics of a novel discrete fractional model for maize streak epidemics with linear control, Int. J. Dyn. Control. 13 (2025) 5.
[37] Wei Lin, Global existence theory and chaos control of fractional differential equations, J. Math. Anal. Appl. 332 (1) (2007) 709–726.
[38] A. El-Mesady, Nauman Ahmed, Amr Elsonbaty, Waleed Adel, Transmission dynamics and control measures of reaction–diffusion pine wilt disease model, Eur. Phys. J. Plus 138 (2023) 1078.
[39] Waleed Adel, H.M. Srivastava, M. Izadi, A. El-Mesady, Dynamics and numerical analysis of a fractional-order toxoplasmosis model incorporating human and cat populations, Bound. Value Probl. 2024 (152) (2024).
[40] Bright Elisamehe, Augustino Isdory Msigwa, Expeditho L. Mtisi, Nyimvua Shaban Mbare, Modeling the impact of integrated intervention strategies on early blight dynamics in tomato crops, Sci. Afr. (2025) e02778.
[41] B.Z. Naaly, T. Marijani, A. Isdory, J.Z. Ndendya, Mathematical modeling of the effects of vector control, treatment and mass awareness on the transmission dynamics of dengue fever, Comput. Methods Programs Biomed. Updat. 6 (2024) 100159.
[42] J.Z. Ndendya, G. Mlay, H. Rwezaura, Mathematical modelling of COVID-19 transmission with optimal control and cost-effectiveness analysis, Comput. Methods Programs Biomed. Updat. 5 (2024) 100155.
[43] Sylas Oswald, Mathematical Modelling of Bovine Tuberculosis Transmission Dynamics with Optimal Control of Some Control Measures, (M.Sc. in Mathematical Modelling Thesis), University of Dar es Salaam, Dar es Salaam, Tanzania, 2023.
[44] T. de-Camino-Beck, M.A. Lewis, P. Van den Driessche, A graph-theoretic method for the reproduction number in continuous time epidemiological models, J. Math. Biol. (2009) 503–516.
[45] T. de-Camino-Beck, M.A. Lewis, On net reproductive rate and the timing of reproductive output, Amer. Nat. 172 (1) (2008) 128–139.
[46] T. de-Camino-Beck, M.A. Lewis, A new method for calculating net reproductive rate from graph reduction with applications to the control of invasive species, Bull. Math. Biol. 69 (2007) 1341–1354.
[47] C.K. Li, H. Schneider, Applications of Perron–Frobenius theory to population dynamics, J. Math. Biol. 44 (5) (2002) 450–462.
[48] J.P. La Salle, The Stability of Dynamical Systems, Society for Industrial and Applied Mathematics, 1976.
[49] H.I. Freedman, S. Ruan, M. Tang, Uniform persistence and flows near a closed positively invariant set, J. Dynam. Differential Equations (1994).
[50] M.Y. Li, Z. Shuai, Global-stability problem for coupled systems of differential equations on networks, J. Differential Equations 248 (1) (2010) 1–20.
[51] T. Kuniya, Global stability analysis with a discretization approach for an age-structured multigroup SIR epidemic model, Nonlinear Anal. Real World Appl. 12 (5) (2011) 2640–2655.
[52] H. Guo, M.Y. Li, Z. Shuai, Global stability of the endemic equilibrium of multigroup SIR epidemic models, Can. Appl. Math. Q. 14 (3) (2006) 259–284.
[53] J.Z. Ndendya, L. Leandry, A.M. Kipingu, A next-generation matrix approach using Routh–Hurwitz criterion and quadratic Lyapunov function for modeling animal rabies with infective immigrants, Heal. Anal. 4 (2023) 100260.
[54] E. Hairer, C. Lubich, M. Schlichte, Fast numerical solution of nonlinear Volterra convolution equations, SIAM J. Sci. Stat. Comput. 6 (3) (1985) 532–541.
[55] J.I. Irunde, J.Z. Ndendya, J.A. Mwasunda, P.K. Robert, Modeling the impact of screening and treatment on typhoid fever dynamics in unprotected populations, Results Phys. 54 (2023) 107120.
[56] Tanzania Basic Demographic and Socio-Economic profile, Tanzania basic demographic and socio-economic profile, 2024, (Accessed 27 November 2024).
[57] T. Malik, J. Reimer, A. Gumel, E.H. Elbasha, S. Mahmud, The impact of an imperfect vaccine and pap cytology screening on the transmission of human papillomavirus and occurrence of associated cervical dysplasia and cancer, Math. Biosci. Eng. 10 (4) (2013) 205–1173.
[58] P.K. Rajan, M. Kuppusamy, O.F. Egbelowo, A mathematical model for human papillomavirus and its impact on cervical cancer in India, J. Appl. Math. Comput. 69 (1) (2023) 753–770.
[59] Mlyashimbi Helikumi, Paride O. Lolika, Steady Mushayabasa, Analysis of Caputo fractional-order model for COVID-19 with non-pharmaceuticals interventions and vaccine hesitancy.
[60] Simeone Marino, Ian B. Hogue, Christian J. Ray, Denise E. Kirschner, A methodology for performing global uncertainty and sensitivity analysis in systems biology, J. Theoret. Biol. 254 (1) (2008) 178–196.
[61] Stefan Banach, Sur les opérations dans les ensembles abstraits et leur application aux équations intégrales, Fund. Math. 3 (1) (1922) 133–181.
[62] Sanaa L. Khalaf, Mohammed S. Kadhim, Ayad R. Khudair, Studying of COVID-19 fractional model: Stability analysis, Partial. Differ. Equ. Appl. Math. 7 (2023) 100470.
[63] Roberto Garrappa, Predictor-corrector PECE method for fractional differential equations, 2011, MATLAB Central File Exchange.
[64] Gerardus Polla, Comparing accuracy of differential equation results between Runge-Kutta Fehlberg methods and Adams-Moulton methods, Appl. Math. Sci. 7 (2013) 5115–5127.
[65] Lingbo Zhang, Studying and Comparing Numerical Methods for Ordinary Differential Equations.
[66] K. Diethelm, N.J. Ford, A.D. Freed, Detailed error analysis for a fractional Adams method, Numer. Algorithms 36 (1) (2004) 31–52.
[67] K. Diethelm, Efficient solution of multi-term fractional differential equations using P(EC)mE methods, Computing 71 (2003) 305–319.
[68] Mlyashimbi Helikumi, Thobias Bisaga, Kimulu Ancent Makau, Adquate Mhlanga, Modeling the impact of human awareness and insecticide use on malaria control: A fractional-order approach, Mathematics 12 (22) (2024) 3607.
[69] Kai Diethelm, Alan D. Freed, The FracPECE subroutine for the numerical solution of differential equations of fractional order, Forsch. Und Wiss. Rechn. 1999 (1998) 57–71.
[70] S. Praveena, S.M. Pavithra, A.D.V. Dalvin Vinoth Kumar, P. Veeresha, CNN-based Indian medicinal leaf type identification and medical use recommendation, Neural Comput. Appl. 36 (10) (2024) 5399–5412.
[71] Anwarud Din, Yongjin Li, Optimizing HIV/AIDS dynamics: stochastic control strategies with education and treatment, Eur. Phys. J. Plus 139 (9) (2024) 1–19.
[72] Anwarud Din, Bifurcation analysis of a delayed stochastic HBV epidemic model: Cell-to-cell transmission, Chaos Solitons Fractals 181 (2024) 114714.
[73] Qura Tul Ain, Nonlinear stochastic cholera epidemic model under the influence of noise, J. Math. Tech. Model. 1 (1) (2024) 52–74.
[74] Shafi Ullah, Investigating a coupled system of Mittag-Leffler type fractional differential equations with coupled integral boundary conditions, J. Math. Tech. Model. 1 (2) (2024) 16–28.